AIMS Biophysics

AIMS Biophysics, 12(1): 69−100.
DOI: 10.3934/biophy.2025006
Received: 23 December 2024
Revised: 22 February 2025
Accepted: 06 March 2025
Published: 13 March 2025

http://www.aimspress.com/journal/biophysics

*Review*

# Subcutaneous sustained-release drug delivery system for antibodies and proteins

**Takayuki Yoshida* and Hiroyuki Kojima**

Pharmaceutical Research and Technology Labs., Astellas Pharma Inc., 180, Ozumi, Yaizu, Shizuoka, 425-0072 Japan

* **Correspondence:** Email: takayuki.yoshida@astellas.com; Tel: +818013150631.

**Abstract:** Subcutaneous (SC) sustained release is an important drug delivery system (DDS) for antibody/protein drugs because it reduces dosing frequency. This review discusses formulations and biophysical parameters that affect the pharmacokinetics (PK) of DDSs. For example, SC injectable microspheres and polymeric hydrogels, as well as intradermal microneedles, suppress denaturation in loading and burst release of drugs [growth hormone, interferon-α2b, bevacizumab, and single-chain antibody fragment (scFv)]. These DDSs significantly prolong half-life ($t_{1/2}$) in plasma with low maximum concentration ($C_{max}$) and low relative bioavailability after SC dosing to animals and/or humans. Formulation parameters, such as (1) drug loading amount, (2) drug diffusion in DDS, (3) interactions of drugs with polymers, and (4) microneedle design, likely contribute to their PK profiles. This review also discusses the effects of many biophysical parameters on PK, including (5) in vivo behavior of polymers (swelling, aggregation, dissolution, and accumulation), (6) drug interactions with extracellular matrix and hypodermis diffusion, (7) drug unfolding, (8) hypodermic concentration of drugs, inherent proteins, and cells, (9) drug absorption through lymphatic or blood vessels, (10) degradation of drugs/polymers by proteases/phagocytic cells, (11) FcRn-mediated recycling, (12) FcγR-mediated endocytosis, and (13) target-mediated drug clearance. For safe dosing, (14) skin's thickness/viscoelastic properties and variations and (15) skin's recovery are also important factors. Consideration of these effects will increase the developmental speed and success of many SC sustained-release DDSs of antibody/protein drugs.

**Keywords:** drug delivery system; sustained release; antibody; protein; subcutaneous; microneedle

## 1. Introduction

Antibodies and proteins are crucial modalities of pharmaceutically active ingredients in drug development. Compared with small molecule drugs, antibody and protein drugs have a larger molecular size and substantial surface area. This allows selective binding to target molecules and, in turn, provides high specificity in reducing off-target adverse effects [1,2]. Antibodies can target protein–protein interactions, whereas small molecules cannot. When the molecular mechanisms of a disease and the target molecules involved in its pathogenesis are identified, protein drugs can directly replace deficient or abnormal target proteins, and antibody drugs can interfere with the target molecules or their interactions [3]. Comparing pharmaceutical clinical trials conducted between 2001 and 2009 and 2015 and 2023, the percentage of small molecule drugs declined from 66% to 47%, while antibodies increased (from 11% to 20%) and proteins/peptides maintained their share (from 9.4% to 9.2%) [1]. Antibodies and proteins/peptides reportedly showed higher success rates in drug clinical development (11% and 5.3%, respectively) compared with small molecule drugs (4.1%) in 2015–2023 [4].

The large molecular size of antibodies and proteins limits penetration across cellular membranes. The low pH in the stomach, enzymes (proteases and peptidases) in the gastrointestinal tract, and first-pass metabolism by cytochrome P450 in the liver and enterocytes cause the denaturation of protein drugs [5]. This very low oral bioavailability restricts administration routes to injections, such as intravenous (IV), subcutaneous (SC), and intramuscular (IM). However, IV/SC/IM dosing is subject to a number of potential risks, including needle phobia, pain, low patient adherence, phlebitis, and tissue necrosis and infection [6,7]. To reduce these risks, sustained-release drug delivery systems (DDSs) can allow a decrease in the frequency of injections. In particular, IV infusion carries a high economic burden in medical care and medication costs. These include longer administration times, high costs to patients due to health personnel and clinical occupancy costs, lost workdays, and patient and caregiver travel expenses [8]. Among the IV/SC/IM route, SC dosing is beneficial for patient comfort and compliance and provides time and money savings [9]. SC dosing does not require premedication and requires only a few minutes compared to the several hours required for IV infusion [9]. SC formulations therefore reduce healthcare professional workload and, in turn, decrease hospital costs [10,11]. Further, patients prefer SC to IV. Also, SC dosing might be safer and have greater tolerance than the IV route in many cases and seems to provide a better health-related quality of life [10,11]. IM dosing carries the risk of nerve damage and improper drug deposition; it can induce pain, swelling, or irritation at the injection site and tissue damage and has limited injection volumes [9]. These comparisons have made SC dosing an attractive alternative to the IV, IM, and oral routes [9]. Recently, SC formulations have gained attention as secondary formulations after IV products. For instance, atezolizumab, an immunoglobulin (IgG) 1 kappa monoclonal antibody (mAb), which binds to programmed death ligand 1 (PD-L1), was first marketed as an IV product and subsequently as a new SC formulation [12]. Even SC formulations for trastuzumab, rituximab, and daratumumab were secondarily developed after IV products [13,14]. Sustained-release SC formulations are considered useful technologies that increase the value of marketed drugs as new formulations in product lifecycle management. Moreover, given that some antibody fragments and proteins have a short half-life ($t_{1/2}$) in blood [15,16], SC sustained-release DDSs are critical to enabling sufficient efficacy and increasing the probability of successful new drug development.

**Table 1.** Formulation and biophysical parameters that can affect a drug's pharmacokinetics and adverse events.

| | No. | Parameter |
|---|---|---|
| Formulation parameters | 1 | Drug loading amount |
| | 2 | Drug diffusion in DDS |
| | 3 | Drug interactions with polymers |
| | 4 | Design of microneedle |
| | 5 | In vivo behavior of polymers (swelling, aggregation, dissolution, accumulation) |
| | 6 | Drug interactions with extracellular matrix and hypodermis diffusion |
| | 7 | Drug unfolding |
| | 8 | Hypodermis concentration of drug/inherent proteins/cells |
| Biophysical parameters | 9 | Absorption through lymphatics or blood vessels |
| | 10 | Degradation of drugs/polymers by proteases/phagocytic cells |
| | 11 | FcRn-mediated recycling |
| | 12 | FcγR-mediated endocytosis |
| | 13 | Target-mediated drug clearance |
| | 14 | Skin thickness/viscoelastic property and individual/site differences |
| | 15 | Skin recovery |

DDS: drug delivery system; FcRn: neonatal fragment; FcγR: Fc gamma receptor

Sustained-release DDS products of small molecule and peptide drugs have been widely established for clinical use. Examples include rods, microspheres, and in situ gel formulations of poly(lactic-co-glycolic acid) (PLGA), as well as Risperdal Consta®, Zoladex®, Lupron Depot®, and Eligard® [17–20]. IV dosing of sustained-release DDS is hampered by the disadvantages of the initial burst drug release by dilution with a large volume of blood and faster systematic elimination through the reticuloendothelial system (liver, spleen, etc.) [21]. IM administration also carries the risks mentioned above. For these reasons, many DDS products that aim for the sustained release of small molecules are administered through the SC route. In contrast to many DDS products of small molecule/peptide drugs, the number of sustained-release DDS for antibody/protein drugs used in clinical practice is limited; examples include Nutropin Depot® [biweekly SC PLGA microsphere of human growth hormone (hGH)] [22] and the INFUSE® bone graft [collagen sponge of recombinant human bone morphogenetic protein-2 (rhBMP-2) in spinal-fusion procedures] [23]. The most challenging points for sustained-release DDS of antibody/protein drugs are drug release control and the maintenance of bioactivity. Among these, the hydrophilicity and high water solubility of antibodies/proteins frequently cause burst drug release. When hydrophobic polymers are used to suppress drug release, their dissolution requires organic solvents, but these in turn affect the conformation and bioactivity of the antibodies/proteins [24]. Most small molecules can rapidly diffuse into the blood without degradation after SC dosing. In contrast, the movement and fate of the DDS and antibody/protein drugs are affected by many formulations and biophysical parameters at the dosing site (Table 1). This review summarizes two kinds of SC dosing of DDS: subcutaneous injection and intradermal microneedle (MN). Several embodiments of sustained-release DDS for antibody/protein drugs are described, including PLGA microspheres for hGH, hydrogel particles for interferon-α2b

(IFNα-2b), amphiphilic copolymer hydrogel for bevacizumab, conjugated hydrogel microspheres for anti-tumor necrosis factor alpha (TNFα) single-chain antibody fragment (scFv), and dissolving/hydrogel MN for bevacizumab. The effects of the formulation and biophysical parameters (Table 1) on the in vivo performance of DDS, such as pharmacokinetics (PK) and adverse events, are also discussed. Information and insights from this paper will lead to improvements in the speed and precision of SC sustained-release DDS, which will in turn expand their application to broader antibody/protein drugs and deliver high value to many patients.

## 2. Subcutaneous injections

The in vivo fate of antibody/protein drugs after SC injection is affected by various biophysical parameters (Figure 1; Table 1). The first is the drug diffusion into the interstitial space of the hypodermis from the injection site. Tissue interstitial fluid accounts for 70% of the total volume of the hypodermis, while the extracellular matrix (ECM) is the main component of the other 30% [25,26]. The fluid is an ultrafiltrate of plasma composed of 97% water and 3% proteins, with a flow on the order of 0.1–2 μm/s [26]. The ECM includes proteoglycans, collagen, elastin, laminin, and fibrin. Due to the large size of antibody/protein drugs and the mesh size and high viscosity of the ECM, drug–ECM interactions significantly reduce the diffusion of the drugs to 18%–93% of their free solution values [26] (Table 1, no. 6). Proteins with a larger size [or molecular weight (MW)] are reported to remain for a longer time at the SC injection site [27]. The time required for a 50% loss of protein from the dosing site was 6.8 h for bevacizumab (MW 149 kDa), 2.85 h for bovine serum albumin (BSA) (MW 66 kDa), 1.57 h for ovalbumin (MW 44.3 kDa), and 0.31 h for vascular epithelial growth factor Cys156Ser (VEGF-C156S) (MW 23 kDa) [28]. Proteoglycan molecules contain highly negatively charged glycosaminoglycan chains, which interact with antibody/protein drugs [29]. Antibodies with high positive charges and hydrophobic interactions reduce absorption rates and bioavailability after SC injection [30] (Table 1, no. 6).

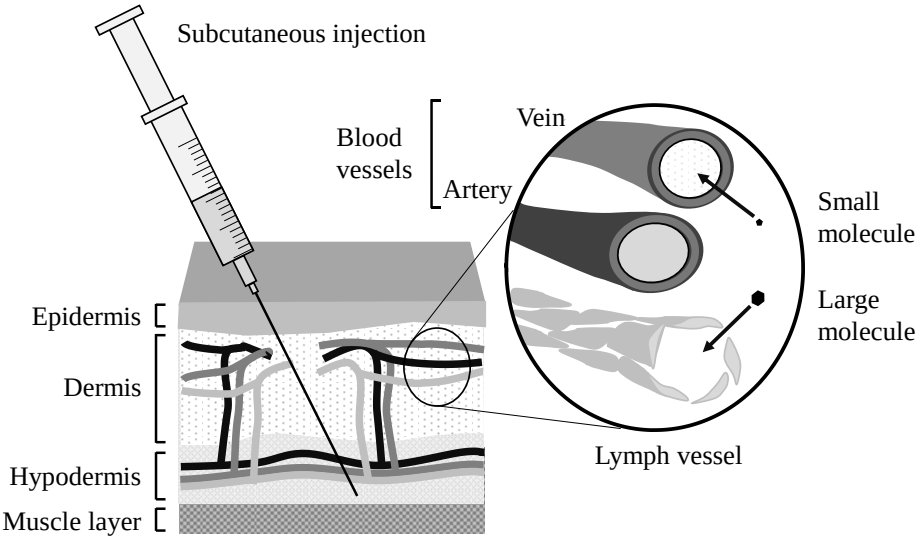


**Figure 1.** Subcutaneous injection and structure of skin, blood, and lymph vessels.

On the other hand, excipients with small molecular sizes, such as histidine, sucrose, and arginine, are frequently used in normal formulations of protein/antibody drugs and diffuse away from the dosing site much faster than antibody/protein drugs [31]. This changes the pH and salt concentration around the drugs after injection, which may in turn cause the precipitation of drug aggregates [32]. These aggregates are retained for a longer time (10–20 h) at the site due to their large size [33–35] (Table 1, no. 6). Moreover, proteases such as matrix metalloproteinases in the hypodermis might degrade antibody/protein drugs (Table 1, no. 10). Degradants of PEGylated erythropoietin (PEG; polyethylene glycol) were observed after incubation with rat subcutaneous tissue homogenate [36]; in contrast, degradation was limited after incubation of bevacizumab, BSA, and ovalbumin with the homogenate [28].

The length of IgG is around 10 nm, while blood capillaries have a pore size of 5–12 nm, and the optimal molecular size for lymphatic uptake is 10–100 nm [37,38] (Figure 1). The lymphatic absorption of molecules with different MW after SC dosing to sheep was as follows [37,39]; 4%, 21%, 17%, 39%, 60%, 62%, 96%, and 99% for 5-fluoro-2'-deoxyuridine (MW 246 kDa), inulin (MW 5.2 kDa), insulin (MW 5.8 kDa), cytochrome c (MW 12.3 kDa), human recombinant IFNα-2a (MW 19.0 kDa), hGH (MW 22 kDa), recombinant human erythropoietin (MW 30 kDa), and darbepoetin α (MW 37 kDa), respectively. This linear relationship (Figure 2) suggests that molecules with MW > 16.5 kDa are absorbed mainly by the lymphatic system (Table 1, no. 9).

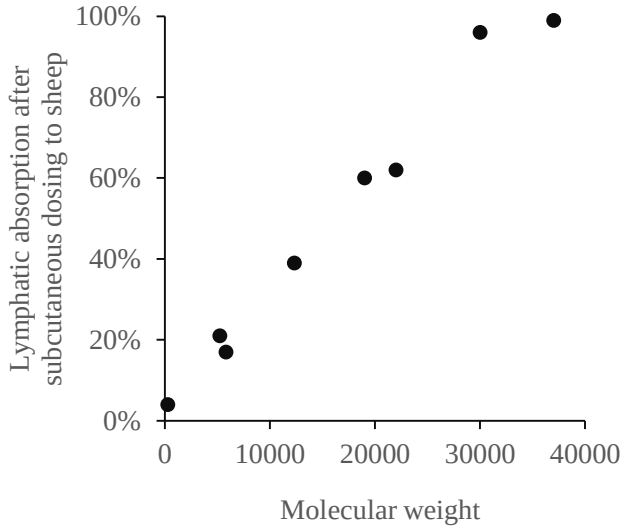


**Figure 2.** Association of protein molecular weight with the percentage of lymphatic absorption after subcutaneous dosing to sheep [37,39].

Once absorbed, antibody/protein drugs are transported to the collecting lymphatics and pass through lymph nodes [29]. Antigen-presenting cells (APCs) in the lymph nodes constantly sample the surrounding medium by micropinocytosis to degrade proteins [27] (Table 1, no. 10). Although antibodies can bind to neonatal fragment crystallizable receptor (FcRn) to escape lysosomal degradation, when binding is saturated at the administered dose, a significant fraction of antibody is catabolized in APC lysosomes (Table 1, no. 11). In previous work, after incubation of proteins with cell suspensions or homogenate of lymph nodes, some portion of PEGylated erythropoietin and

bevacizumab was probably degraded, whereas BSA and ovalbumin were not [28,36]. Although these data may have been affected by a reduction in APC activity or measurement accuracy, catabolism in the lymph nodes appears to vary with the specific antibody/protein involved.

### *2.1. Poly(lactic-co-glycolic acid) microspheres for growth hormone*

Growth hormone (GH or somatotropin) is a single-chain protein containing 191 amino acids (MW 22 kDa) in a four-bundle α-helix protein with no β-sheet structure that is internally cross-linked by two disulfide bonds with an isoelectric point (pI) near 5.3 [40]. GH is secreted episodically from somatotroph cells in the anterior pituitary and stimulates growth and cell reproduction. For patients with GH deficiency, recombinant human GH (rhGH) is the primary treatment. In the 1980s, GH was administered by daily SC injection [41]. However, the plasma $t_{1/2}$ of rhGH is very short, namely 0.36 h after IV dosing and 3.8 h after SC dosing [42,43]. The once-monthly product Nutropin Depot® was approved by the United States Food and Drug Administration (FDA) to provide a more stable blood GH concentration over time and reduce dosing frequency [44,45]. The product consists of PLGA microspheres manufactured using prolease technology, which releases GH gradually.

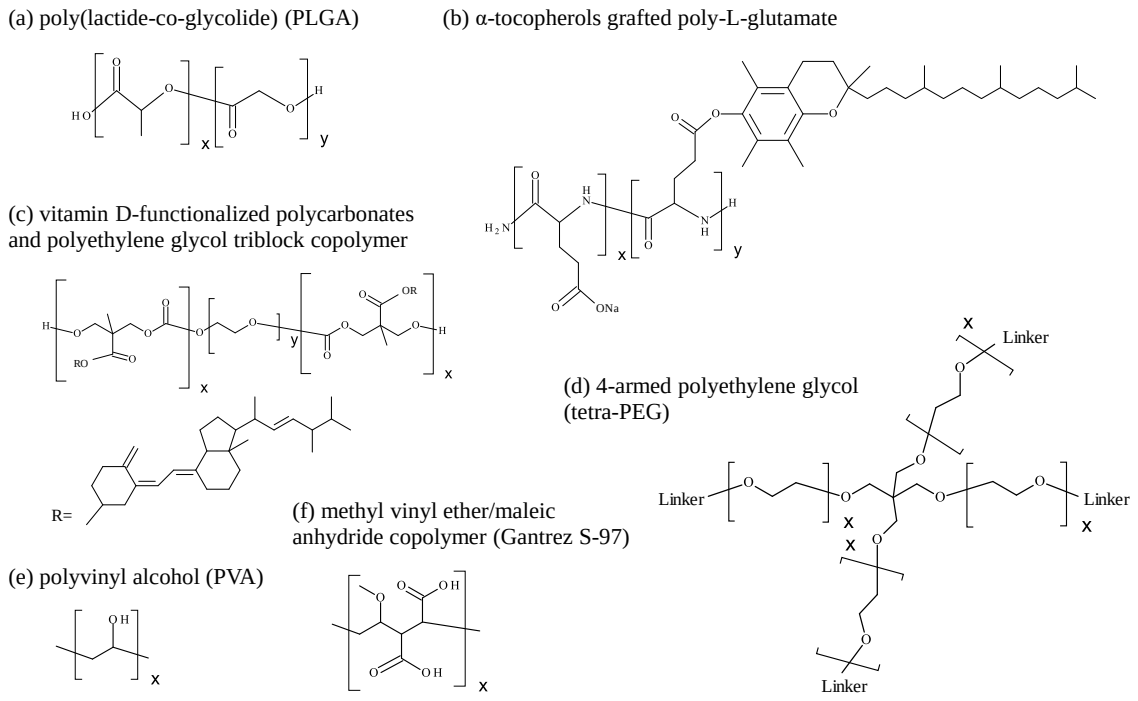


**Figure 3.** Chemical structures of polymers used in drug delivery systems for sustained release of antibodies and proteins.

PLGA is a biodegradable synthetic polymer (Figure 3a). PLGA microspheres are one of the most common sustained-release DDSs for small molecule and peptide drugs, used in Lupron Depot® (leuprolide acetate), Risperidal Consta® (risperidone), and Zilretta® (triamcinolone acetoamide), among others [46–48]. The hydrophobic polymer is dissolved in a volatile organic solvent, commonly dichloromethane, and small molecule or peptide drugs are encapsulated in the microspheres by the oil-

in-water (O/W) or water-in-oil-in-water (W/O/W) solvent evaporation/extraction method. The large interface between the aqueous and organic phases in the emulsification causes the adsorption and denaturation of proteins [49] (Table 1, no. 7). In O/W emulsification of lysozyme aqueous solution with a PLGA dichloromethane solution, a significant amount (20%–37%) of lysozyme was aggregated at the aqueous/organic interface, and protein recovery was found to be irreproducible [49]. Prolease technology aims to avoid the destruction of the tertiary structures of GH and increase encapsulation efficiency using a cryogenic and nonaqueous preparation process. It consists of the following steps: (1) freeze-drying, in which a solution of the drug and excipients is sprayed into liquid nitrogen; (2) dispersal of the drug particles into PLGA organic solution and sonication to reduce particle size; (3) atomization of the suspension into liquid nitrogen to produce frozen microspheres; (4) extraction of the solvent with ethanol; and (5) filtration, vacuum-drying, and sieving to remove large particles [45]. The solvents used in this process (dichloromethane and ethanol) do not dissolve rhGH, resulting in a high encapsulation efficiency of more than 98%.

The microspheres have a median volume diameter of 50 μm and contain 15 wt% of rhGH [42,45] (Table 1, no. 1). Although this drug loading ratio is not high compared with successful examples of PLGA microspheres for peptides/proteins [50], an amount sufficient for microsphere medication containing 18 mg of rhGH can be dispersed in 1 mL of diluent for dosing [51]. The large size of the hydrophobic microspheres can slow polymer degradation, prevent first burst drug release, and suppress diffusion/release rates of the hydrophilic rhGH (Table 1, no. 2). Several assays have confirmed the maintenance of rhGH integrity after processing and release, including a cell proliferation assay that measures rhGH bioactivity. On the other hand, released drugs showed significant aggregation one day after release in a buffer. To stabilize rhGH from denaturation and reduce water solubility to ensure slower release (Table 1, no. 2), a complex of rhGH with zinc (at a molar ratio of 6: 1) was developed. rhGH solubility sharply decreased at a zinc:rhGH molar ratio above 2. The zinc binds at histidine (His)-18 and His-21 on helix 1 and glutamine (Glu)-174 on helix 4 to form a dimer of rhGH [40]. The precipitated rhGH zinc complex maintained the same secondary structure. Conformation of tyrosine and phenylalanine residues was somewhat more rigid, and the angle of the hydrogen bond between aspartic acid (Asp)-169 and tryptophan (Trp)-86 was altered; however, the tertiary structural changes were fully reversible [40], and complete refolding was confirmed in another study. The zinc complex completely prevented the aggregation of proteins released from the microspheres for 28 days [45] (Table 1, no. 7). The zinc complexation also reduced rhGH solubility to minimize the initial burst release. Moreover, sonication of the spray freeze-dried drug particles decreased their size from 10 to 2 μm, reducing the initial release by 25%–33%. PLGA lactide:glycolide monomer ratio (50: 50), carboxyl polymer terminus, and 1% content of zinc carbonate (insoluble salt of a release modifier) were optimized to ensure the most constant serum levels of rhGH and insulin-like growth factor-I (IGF-I) after SC dosing to monkeys. Bioactive hGH stimulated production of IGF-I in vivo [45].

After these improvements to the formulation, manufacturability was also improved, and safety and efficacy were confirmed in preclinical and clinical studies. Nutropin Depot® was approved in 1999. In clinical data from 22 children with GH deficiency [52], a single SC injection of the product (0.75 and 1.5 mg/kg GH dose) provided a serum GH level above baseline for 13–15 days (Table 2). Serum IGF-I levels were also maintained above baseline for 16–20 days [52]. PK modeling estimated that the relative bioavailability of Nutropin Depot® was around 50% (vs. daily rhGH formulations; Table 2). No progressive increase in peak or trough levels of GH were observed after repeated dosing, indicating no accumulation at the dosing site or body [52].

**Table 2.** Pharmacokinetic parameters of growth hormone in humans.

| Formulation | Dosing route | Animal | Dose (mg/kg) | $C_{max}$ (ng/mL) | $t_{1/2}$ (h) | $T_{C>1\ \mu g/mL}$ (days) | Relative bioavailability % (vs. IV) | References |
|---|---|---|---|---|---|---|---|---|
| Humatrope® | IV | human | 0.02 | 415 | 0.36 | - | | [43] |
| Humatrope® | SC | human | 0.1 | 63.3 | 3.8 | ~ 1.3 | 81 | [43] |
| Nutropin Depot® | SC | human | 0.75 | 54 | - | 13 | ~ 50 | [52] |
| Nutropin Depot® | SC | human | 1.5 | 80 | - | 15 | ~ 50 | [52] |

IV: intravenous dosing; SC: subcutaneous dosing; $C_{max}$: maximum concentration; $t_{1/2}$: half-life; $T_{C>1\ \mu g/mL}$: time when growth hormone concentration is greater than 1 μg/mL.

In general, PLGA microspheres are gradually hydrolyzed in the hypodermis after SC dosing [53] (Table 1, no. 5). The biodegradation steps include hydrolytic chain cleavage on their surface, pore diffusion, erosion, and autocatalysis by carboxylic end groups [53,54]. The initial PK profile can be interpreted to mean that rhGH on the microsphere surface was rapidly dissociated, and the initial burst drug release by this surface degradation lasted approximately 48 h [52] (Table 1, no. 5). The long-term sustained GH level was probably caused by subsequent disintegration of the microspheres providing sustained drug release [52]. rhGH is a small anionic inherent protein (pI = 5.3, MW 22 kDa), consequently less likely to interact with the ECM. Its diffusion in the hypodermis was probably rapid (as described in Section 2, Table 1, no. 6). After being released, the rhGH might adsorb on the microspheres to cause unfolding (Table 1, no. 7). Adsorption of rhGH on PLGA nanoparticles was reported in a pH 7.2 buffer [55]. The pI of rhGH is 5.3, and PLGA has anionic charges; accordingly, this adsorption appears to be primarily attributable to hydrophobic interaction. Loss of the tertiary structure of adsorbed rhGH has been suggested, and entropic gain for the unfolding appears to be a primary driving force for adsorption [55]. In the physiological environment, it is unknown whether this adsorption actually occurs or whether the unfolding is reversible or not. It is possible that this adsorption and unfolding might contribute to decreased or slower GH release and low bioavailability.

The lymphatic absorption of rhGH was 62% [37] (Table 1, no. 9), suggesting the possibility that APCs might degrade the rhGH in the lymph nodes (Table 1, no. 10). After intratracheal dosing of fluorescein isothiocyanate (FITC)-labeled hGH to rats [56], rapid and significant uptake of hGH into alveolar macrophages was observed [56,57]. The large microparticle size of this product requires a large-diameter 21 G needle (outer diameter 0.813 mm, inner diameter 0.495 mm) for injection [46]. The main adverse events are related to the injection site, including nodules (60% of injections), erythema (54%), and postinjection pain (36%) [42] (Table 1, no. 15). Generally speaking, dosing of sustained-release DDS and PLGA microspheres causes acute and chronic inflammation, granulation tissue formation, foreign body reaction, and fibrous encapsulation in sequence at the administration site [53,58]. Inflammatory cells respond to the microspheres and the mechanical injury created by injection. Monocytes migrate and differentiate into macrophages to form foreign body giant cells at the microsphere surface. Fibroblasts infiltrate and secrete collagen to form a fibrous capsule surrounding the implant site. Before full degradation, these adverse events are probably caused primarily by reaction to the microspheres and also by injury by the large-diameter needle [42,46,58].

The accumulation of macrophages around the microspheres and in the lymph nodes might take up some portion of the released rhGH, which might cause low bioavailability (Table 1, no. 10).

*2.2. Hydrogel particles for interferon α-2b*

Human IFNα-2b is a glycoprotein cytokine consisting of 166 amino acids (MW 19.2 kDa) with five α helices, two di-sulfide bridges, and an O-glycosylated threonine (Thr)-106 with a pI around 5.9 [59]. IFNα-2b is produced by leukocytes during viral infection. It has wide biological activity and is used in hepatitis and cancer treatments. Plasma $t_{1/2\beta}$ of IFNα-2b after IV and SC injection in humans is approximately 1.7 h and 2.9 h, respectively [60] (Table 3). IFNα-2b has a relatively small therapeutic index, and a high dose causes substantial toxicity [61]. To reduce dosing frequency and control drug plasma concentration level, weekly IFNα-2bXL has been developed using the Medusa hydrogel sustained-release DDS.

**Table 3.** Pharmacokinetic parameters of interferon α-2b.

| Formulation | Dosing route | Animal | Dose | $C_{max}$ (ng/mL) | $t_{1/2}$, $T_{50\%AUC}$, or $T_{SA}$ | Relative bioavailability % (vs. IV) | References |
|---|---|---|---|---|---|---|---|
| Normal solution | IV | human | 5 x $10^6$ IU/$m^2$ | 188 | $t_{1/2\alpha}$ = 0.1 h, $t_{1/2\beta}$ = 1.7 h | | [60] |
| Normal solution | SC | human | 5 x $10^6$ IU/$m^2$ | 55.3 | $t_{1/2\beta}$ = 2.9 h | > 100 | [60] |
| Normal solution | SC | rat | 60 μg/kg | 1.5 | $T_{50\%AUC}$ = 1.4 h, $T_{SA}$ = 0.5 day | - | [62] |
| IFNα-2bXL (Medusa gel) | SC | rat | 60 μg/kg | 27.9 | $T_{50\%AUC}$ = 16.8 h, $T_{SA}$ = 2 days | 58 | [62] |
| Normal solution | SC | dog | 60 μg/kg | 1.4 | $T_{50\%AUC}$ = 4.3 h, $T_{SA}$ = 1 day | - | [62] |
| IFNα-2bXL (Medusa gel) | SC | dog | 60 μg/kg | 28 | $T_{50\%AUC}$ = 39 h, $T_{SA}$ = 4 days | 43 | [62] |
| Normal solution | SC | monkey | 60 μg/kg | 3.4 | $T_{50\%AUC}$ = 3.1 h, $T_{SA}$ = 1 day | - | [62] |
| IFNα-2bXL (Medusa gel) | SC | monkey | 60 μg/kg | 59.6 | $T_{50\%AUC}$ = 30 h, $T_{SA}$ = 6 days | 53 | [62] |
| Viraferon® | SC | human | 3 MIU | 32 | $T_{SA}$ = 1 day | - | [62] |
| IFNα-2bXL (Medusa gel) | SC | human | 18 MIU | 23 | $T_{SA}$ > 7 days | - | [62] |

IV: intravenous dosing; SC: subcutaneous dosing; IU: international units; MIU: million international units; $C_{max}$: maximum concentration; $t_{1/2\alpha}$: half-life during distribution phase; $t_{1/2\beta}$: half-life during terminal elimination phase; $T_{50\%AUC}$: time required for 50% of total area under the curve (AUC); $T_{SA}$: time when interferon-α2b is absorbed; $T_{max}$: time to maximal concentration.

The Medusa technology uses a polymer consisting of a hydrophilic poly-L-glutamate backbone

and grafted hydrophobic α-tocopherols [62] (Figure 3b). The glutamate chains aggregate via the self-assembly of α-tocopherol groups to form hydrogel nanoparticles. The polymer can interact with drugs in the nanoparticles and release them in a sustained manner. SC dosing of the Medusa hydrogel nanoparticles also showed in vivo sustained absorption of IFNα-2b and interleukin-2 (IL-2) in nonclinical and clinical studies [62]. Simple mixing of two aqueous solutions of IFNα-2b and the polymer causes physical binding of the protein to the particles without the use of an organic solvent (Table 1, no. 3). An excess amount of BSA fully displaces the IFNα-2b, and the displaced drug retains the same retention time on HPLC and bioactivity as the native protein [62]. After single SC injection to rats, dogs, and monkeys, IFNα-2bXL prolonged in vivo release by 4, 4, and 6 times compared with normal IFNα-2b solution, respectively (Table 3). The nanoparticles produced a decrease in maximum concentration ($C_{max}$) to around 5% that of the normal solution and showed 43%–58% relative bioavailability to it [62] (Table 3). In a Phase I/II study in 53 patients [63], the absorption time of the immediate formulation of Viraferon® and IFNα-2bXL were 1 day and more than 7 days, respectively. The IFNα-2bXL reduced $C_{max}$ to 10% (Table 3) and reduced the rate of adverse events to 3.7%, compared to 5.2% for Viraferon® [62,63].

Poly-L-glutamate (MW 10.0–16.9 kDa) is used in this technology [64]; each particle contains 10–15 polymer chains and the product contains IFNα-2b 0.3 mg/mL and 23 mg/mL of the polymer [62]. It was therefore calculated that 14% of particles in the product contained one IFNα-2b molecule and that 86% of particles were empty, without any proteins. Since one IFNα-2b molecule (MW 19.2 kDa) was surrounded by 9–14 polymer molecules (MW 10.0–16.9 kDa), the release of the IFNα-2b is probably quite restricted (Table 1, no. 1). The Medusa hydrogel nanoparticles have a small size of 20–50 nm, and drug diffusion in the particles can be neglected (Table 1, no. 2). Regarding the drug–polymer interaction, the poly-L-glutamate might have high affinity with a conformation of the IFNα-2b (Table 1, no. 3). This Medusa hydrogel particle has also shown in vivo sustained release of different protein drugs of IL-2 and hGH [62,64]. After SC dosing of IL-2 to rats, dogs, and monkeys, release time was prolonged by about 1.5 times compared with the immediate release product of Proleukin® (Table 4). In a Phase I/II study in renal carcinoma patients, a single SC injection of Medusa particle suspension extended $T_{> 5\ ng/mL}$ (time when serum IL-2 concentration is greater than 5 ng/mL) by 2.3 times, and time to maximal concentration ($T_{max}$) by 16 times compared with Proleukin® [62] (Table 4). In SC dosing of hGH to dogs [64], this technology extended $T_{> 5\ ng/mL}$ by 7 times and $T_{50\%AUC}$ (time required for 50% of total hGH area under the curve, AUC) by 30 times compared with the immediate release solution [62] (Table 5). The effect of this technology on the PK profiles of the three protein drugs was similar. Regarding the biophysical properties of the three proteins, their pIs are different (6.8, 5.9, and 5.3 for IL-2, IFNα-2b, and hGH, respectively); however, they similarly have slight negative charges in the hypodermis at pH 7.4. Poly-L-glutamate has a low pI of 3.9 and exerts a strong negative charge on the particles, raising little concern about ionic interactions or unfolding of the drugs (Table 1, no. 3 and 7). The three proteins have similar sizes (MW 19.2, 15.5, and 22 kDa for IFNα-2b, IL-2, and hGH) and similar tertiary structures. hGH and IL-2 have the same up-up-down-down four-helix bundle motif [65] (Figure 4), and the topology of IFNα-2b resembles it [66]. This motif is classically viewed as an α-helical coiled coil [67], and poly-L-glutamate tracts have been reported to affect the coiled-coil regions and stabilize protein interactions [68]. These protein structures and interactions might contribute to their sustained release from the Medusa particles (Table 1, no. 3).

**Table 4.** Pharmacokinetic parameters of interleukin-2 after dosing of Medusa hydrogel or Proleukin®.

| Formulation | Dosing route | Animal | Dose (IU/m$^2$) | $C_{max}$ | $T_{SA}$ (days) | $T_{max}$ (h) | $T_{C>5\ ng/mL}$ (h) | Relative bioavailability % (vs. IV) | References |
|---|---|---|---|---|---|---|---|---|---|
| IL-2XL (Medusa gel) | SC | rat | unreported | 1/100 of Proleukin | 3 (Proleukin: 2) | - | - | 10 | [62] |
| IL-2XL (Medusa gel) | SC | dog | unreported | 1/13 of Proleukin | 5 (Proleukin: 3) | - | - | 40 | [62] |
| IL-2XL (Medusa gel) | SC | monkey | unreported | 1/2 of Proleukin | 3–4 (Proleukin: 2–3) | - | - | 100–150 | [62] |
| Proleukin® | SC | human | $10.6 \times 10^6$ | ~ 5.3 | - | 2–4 | 3 | - | [62] |
| IL-2XL (Medusa gel) | SC | human | $10.6 \times 10^6$ | ~ 1.6 | - | 48 | 7 | - | [62] |

IV: intravenous dosing; SC: subcutaneous dosing; IU: international units; $C_{max}$: maximum concentration; $T_{SA}$: time when interferon α-2b is absorbed; $T_{max}$: time to maximal concentration; $T_{C>5\ ng/mL}$: time when drug concentration is greater than 5 ng/mL.

**Table 5.** Pharmacokinetic parameters of growth hormone in dogs.

| Formulation | Dosing route | Animal | Dose (mg/kg) | $C_{max}$ (ng/mL) | $T_{C>5\ ng/mL}$ (h) | $T_{50\%AUC}$ (h) | References |
|---|---|---|---|---|---|---|---|
| Normal solution | SC | dog | 1 | 582 | 18 | 4 | [64] |
| Medusa gel | SC | dog | 1 | 25 | 129 | 121 | [64] |

SC: subcutaneous dosing; $C_{max}$: maximum concentration; $T_{C>5\ ng/mL}$: time when drug concentration is greater than 5 ng/mL; $T_{50\%AUC}$: time required for 50% of total AUC.

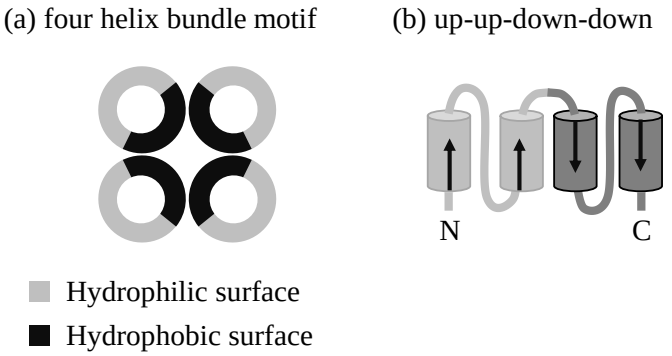


**Figure 4.** Tertiary structures of proteins.

In hypodermis, the poly-L-glutamates might stably aggregate for an extended period (Table 1, no. 5). Research into the solution-state structures of poly-L-glutamates of 10–20 residues revealed that longer residues increased peptide-peptide hydrogen-bonding contacts and β-strand-like conformation and induced aggregation [69]. Poly-L-glutamates of more than 36 residues long in huntingtin protein are observed in Huntington's disease patients. This aggregation is associated with the faster onset of symptoms [69]. With the Medusa technology, the proportion of grafted tocopherol is 5.1 mol% [64], and the poly-L-glutamate (MW 16.9 kDa) is calculated to contain 130 residues, with an average number of glutamate residues between the tocopherol groups of around 26. Therefore, strong polymer aggregation might contribute to the stable adsorption and sustained release of some protein drugs. Moreover, α-tocopherol may also contribute to the in vivo stability of the polymer (Table 1, no. 5). With regard to α-tocopherol hydrophobic nanodomains, the aggregation number of D-α-tocopheryl polyethylene glycol succinate (TPGS) micelles (number of surfactant molecules in a micelle) is > 100; this is higher than those of other nonionic amphiphiles and is caused by the dense packing of tocopherol moieties within the core [70]. In the Medusa particles, 10–15 α-tocopherol moieties were assembled, probably due to steric hindrance from the polymer length; however, the dense packing of 10 nanodomains/particle probably contributes to the high stability of the particles and the slow water penetration and sustained degradation of the particle [62]. The high stability of the Medusa hydrogel likely helped the sustained drug release in hypodermis.

Drug release from the hydrogel may be influenced by the hypodermal concentration of inherent BSA (Table 1, no. 8). In an in vitro study, approximately 80% of IFNα-2b was displaced by BSA (MW 66.5 kDa) at [BSA]/[polymer] weight ratio = 10, molar ratio = 2.5 [62]. This suggested that 220 BSA molecules were necessary for the displacement of one IFNα-2b molecule. Comparison of the interstitial albumin concentration (7.36 mg/mL) in human adipose tissue [71] and the polymer concentration of the product (23 mg/mL) also imply a limited in vivo displacement, and this might contribute to sustained release and absorption. After release, IFNα-2b is an anionic and small-sized protein (pI = 5.9, MW 19.2 kDa); as a consequence, it probably did not interact with the ECM, and its hypodermis diffusion was fast (as described in Section 2, Table 1, no. 6). The released IFNα-2b maintained bioactivity, confirming that its folding was correct. The first reason is the mild preparation process for the hydrogel with mixing of the aqueous solutions only. Further, the biocompatible poly-L-glutamates with a negative charge (pI of the polymer = 3.9) probably contribute to the maintenance of IFNα-2b's tertiary structure (Table 1, no. 7). The lymphatic absorption of IFNα-2b is estimated to

be approximately 60% (Table 1, no. 9) from the linear correlation (Figure 2), indicating the possibility of drug degradation by APCs in the lymph nodes. Moreover, in the hypodermis, Medusa's polymer is degraded by macrophages [62], and many APCs are probably recruited around the hydrogel. After repeated SC dosing of the hydrogel in rats and monkeys, low-grade inflammation was observed at the injection site [62]. Primarily mononuclear cells, lymphocytes, and/or foamy macrophages were gathered at the cutis and/or subcutis of the site. In the absorption of IFNα-2b, APCs in the hypodermis and the lymph nodes might degrade IFNα-2b to cause sustained absorption and low bioavailability (Table 1, no. 10).

### *2.3. Amphiphilic copolymer hydrogel for bevacizumab*

Bevacizumab is a recombinant humanized anti-VEGF-A monoclonal IgG1 antibody (MW 149 kDa) with pI = 8.3 [72]. Bevacizumab specifically binds to VEGF-A, which interacts with VEGF receptor (VEGFR)-1 and VEGFR-2 and inhibits angiogenesis and tumor growth. It is used in the treatment of various cancers, including metastatic colorectal cancer, non-small cell lung cancer, metastatic renal cell carcinoma, cervical cancer, ovarian/fallopian tube/peritoneal cancer, glioblastoma, and metastatic hepatocellular carcinoma [73]. IV infusion of bevacizumab to patients showed an initial half-life $t_{1/2\alpha}$ of 1.4 days and a terminal half-life $t_{1/2\beta}$ of 20 days [74] (Table 6). Biweekly infusion of 30–90 min places a high cost and burden on patients and health personnel, and a sustained-release DDS for bevacizumab has been investigated [75–80].

In one study, a physically cross-linked hydrogel of ABA triblock amphiphilic copolymers was used for delivery [75]. The polymer's A and B blocks were vitamin D-functionalized polycarbonates (V) and PEG (MW 20 kDa), respectively (V-PEG-V) (Figure 3c). The preparation step of the hydrogel involved the addition of bevacizumab aqueous solution to the polymer only. Hydrogel containing 5 wt% polymer allowed quick and easy injection through a 23 G needle and demonstrated a shear-thinning property for recovery of a solid-like state to control drug release after injection. This formulation released the monoclonal antibody (mAb) gradually in a dissolution test. In an efficacy evaluation of a single dose of bevacizumab in tumor-bearing mice, IV and intraperitoneal injections of mAb normal solution showed no efficacy against tumor progression. In contrast, SC injection of the hydrogel remarkably reduced tumor growth [75]. After SC dosing of fluorophore-labeled bevacizumab hydrogel, the mAb was localized to the injection site and gradually decreased with time. In the bevacizumab PK profile after IV dosing of the solution, $C_{max}$ was 4.5 μg/mL, $t_{1/2\alpha}$ was 2–6 days, and the concentration decreased to 0.6 μg/mL at 14 days [75] (Table 6). In contrast, the hydrogel SC dosing maintained a constant bevacizumab plasma level (0.5–1.0 μg/mL) for 1–21 days [75] (Table 6). Bioavailability of the SC V-PEG-V hydrogel was estimated to be 50%–70% [75], which was lower than that of the SC bevacizumab solution (> 100%) in another study [81] (Table 6).

**Table 6.** Pharmacokinetic parameters of bevacizumab after dosing in humans and mice.

| Formulation | Dosing route | Animal | Dose (mg/kg) | $C_{max}$ (μg/mL) | $t_{1/2\alpha}$ | $t_{1/2\beta}$ (days) | Characteristics for sustained absorption | Relative bioavailability % (vs. IV) | References |
|---|---|---|---|---|---|---|---|---|---|
| Normal solution | IV | human | 5 | 125 | 1.4 days | 20 | - | | [74] |
| Avastin® | IV | mouse | 5 | ~ 4.5 | 2–6 days | - | - | 100 | [75] |
| V-PEG-V hydrogel | SC | mouse | 5 | ~ 1.0 | - | - | constant 0.5–1.0 μg/mL for 1–21 days | ~ 50–70 | [75] |
| Normal solution | IV | mouse | 9.3 | 174 | 1.2 h | 6.8 | - | 100 | [81] |
| Normal solution | SC | mouse | 9.3 | 74.1 | 6.2 h | 6.1 | - | > 100 | [81] |

IV: intravenous dosing; SC: subcutaneous dosing; $C_{max}$: maximum concentration; $t_{1/2\alpha}$: half-life during distribution phase; $t_{1/2\beta}$: half-life during terminal elimination phase.

Regarding the in vitro bevacizumab release from the V-PEG-V hydrogel (Table 1, no. 2), an initial burst release was not observed, and 65% and 80% of the drug was released in 5 and 9 days, respectively [75]. Hydrogels containing 4, 5, and 6 wt% polymer showed storage moduli (G') in proportion to concentration and the same release profiles, which suggested that differences in gel stiffness and porosity did not affect drug diffusion in the polymeric network. Since the hydrodynamic radius of mAb (about 7 nm) is smaller than the pore size of the hydrogels (2–20 μm diameter), the network might not act as a diffusion barrier, and the sustained release may be associated with physical interactions between the polymer and mAb (Table 1, no. 3). Another study reported the release profile of tenofovir (MW 476) from the same V-PEG-V hydrogel [82]. Tenofovir is an analog of adenosine monophosphate with an aqueous solubility around 2.5 mg/mL. In the dissolution test, 40% and 80% of tenofovir were released in 0.1 and 2 h, respectively. Although the test conditions were slightly different, the discrepancy in 80% release time between 9 days (bevacizumab) and 2 h (tenofovir) was significant. The in vivo retention of bevacizumab, at about 50% and 25% of the mAb in the dosing site at 2 and 6 days after SC dosing, is similar to the in vitro release profile. Regarding drug solubility, a 100–200 mg/mL mAb

aqueous solution without either organic solvents or surfactants is used in several products administered to patients [83]. Accordingly, the water solubility of mAbs is generally high, and solubility likely does not explain the slow release of bevacizumab. In another study, a hydrogel of a similar triblock copolymer gradually released trastuzumab in a dissolution test [84]. In the polymer, vitamin D-functionalized polycarbonates of V-PEG-V were replaced with vitamin E-functionalized polycarbamates. Trastuzumab release showed no initial burst release, and 40% and 60% of the drug was released in 10 and 42 days, respectively [84]. The carbonate and carbamate moieties of the polymers can form hydrogen bonds with amide bonds of the loaded mAb, which might contribute to a sustained release (Table 1, no. 3).

Regarding the degradation process of the hydrogel (Table 1, no. 5), intact hydrogel remained at 4 days after SC dosing in mice. Gel thickness was noticeably reduced at 1 week, and the hydrogel was completely degraded by 6 weeks [75]. The time course of hydrogel clearance was similar to that of drug retention/clearance at the injection site, which indicated that the in vivo release of bevacizumab was controlled by erosion of the hydrogel [75]. The size of the released bevacizumab is large (MW 149 kDa), and its charge is cationic (pI = 8.3) [72]; accordingly, the drug probably bound with the anionic ECM and slowly diffused in the hypodermis, as described in Section 2 (Table 1, no. 6). In SC dosing of the normal solution to mice, the $t_{1/2}$ of drug clearance from the dosing site (6.8 h) [28] was consistent with the $t_{1/2\alpha}$ of plasma drug level (6.2 h) [81] (Table 6). This may suggest that the absorption rate of SC-dosed bevacizumab solution is mainly dominated by drug diffusion in the hypodermis. Regarding the folding of the released bevacizumab (Table 1, no. 7), an ELISA test using an IgG-Fc antibody detected the drug at 3 weeks post-dosing. Further, its anti-tumor efficacy lasted 2 months. These findings may support the maintenance of the tertiary structure, albeit no clear evidence was obtained [75]. Regarding the absorption routes (Table 1, no. 9), almost all bevacizumab was probably absorbed via the lymphatic route due to its large size (MW 149 kDa, Figure 2). In another study, 17% of bevacizumab's heavy chain was degraded after 24 hour incubation with lymph node homogenate [28]. Since the V-PEG-V hydrogel gradually released the drug in vivo, bevacizumab concentration in the lymph nodes may be lower after dosing of the gel compared with dosing of the normal drug solution. This lower drug concentration might result in the degradation of a more significant portion of the drug by APCs in the lymph nodes and the lower bioavailability of the V-PEG-V hydrogel (Table 1, no. 8 and 10).

The same phenomenon in hypodermis might also contribute to low bioavailability (Table 1, no. 8 and 10). Its shear-thinning property enabled the injection of the hydrogel through a thin needle (23 G), which likely, in turn, caused little inflammation (Table 1, no. 14–15). However, SC dosing of the blank hydrogel resulted in infiltration of some inflammatory cells into the hydrogel [75]. CD45-positive cells include macrophages, dendritic cells, and T cells. Although dendritic cells and T cells might be associated with foreign body reactions, macrophages are central mediators and play key roles in the phagocytosis of injected materials [85]. Macrophages express Fc gamma receptor (FcγR) and the highest level of FcRn [86] (Table 1, no. 11–12). Moreover, uptake by APCs was higher for mAb with a more positive charge [87], and bevacizumab (pI = 8.3) is cationic in the hypodermis [72]. All considered, together with the implications of other studies [5,25,87,88], the presence of many macrophages around the hydrogel might reduce the $C_{max}$ and bioavailability of bevacizumab in the following manner: at a high concentration of bevacizumab, the free fraction of FcRn in macrophages is decreased. A significant fraction of bevacizumab cannot be recycled by binding to FcRn but rather binds to FcγR and is degraded in lysosomes (Figure 5). If the concentration of bevacizumab in

hypodermis after normal solution dosing >> FcγR capacity > the concentration after gel dosing > FcRn capacity, then FcγR-mediated degradation would be negligible in the normal solution but would be more significant in the sustained-release hydrogel (Table 1, no. 8 and 11–12).

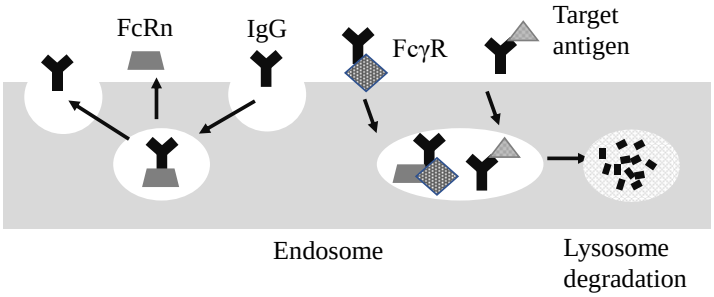


**Figure 5.** Recycling and degradation of antibody.

This lower bioavailability might also be associated with target-mediated clearance (Table 1, no. 13). After mAb binds to the target antigen, the complex may be internalized and degraded in lysosomes [5] (Figure 5). For example, clearance was shown to be important for alemtuzumab (mAb targeting CD52) [89], evolucumab (mAb targeting protein convertase subtilisin kexin type 9: PCSK9) [90], and mAbs targeting high-density and rapidly internalized antigens such as human epidermal growth factor receptor-2 (HER2) [91]. In bevacizumab treatment for patients, bevacizumab serum concentration is approximately 200–400 μg/mL (corresponding to 1–3 μM), and VEGF levels were 0.4–3 pM and 0.3–3 pM in plasma and interstitial muscle of humans, respectively [92]; therefore, the contribution of target-mediated clearance to the overall clearance of bevacizumab was probably insignificant [93]. Similar hypodermis VEGF level was estimated in HCT116 cell-bearing mice, used in the efficacy evaluation of V-PEG-V hydrogel [75], from reported data of plasma VEGF (50 pg/mL, 1.1 pM) in similar mice [94]. On the other hand, a significant effect of the target-mediated clearance on PK has been reported at a low dose of a mAb (2F8) against epidermal growth factor receptor (EGFR) [95]. While a single IV dose of the mAb (2F8) to cynomolgus monkeys showed similar elimination of plasma concentration at 40 and 20 mg/kg, clearance was 3–4 times faster at 2 mg/kg [95]. These findings suggest that the clearance route was negligible at higher mAb plasma levels but became dominant at low plasma levels. mAb (2F8) plasma concentration was 0.2–67 μg/mL at a 2–20 mg/kg dose [95]. Plasma bevacizumab levels were low (approximately 1 μg/mL) after dosing the V-PEG-V hydrogel [75]. These comparisons might suggest that target-mediated clearance plays an important role under a low bevacizumab concentration in plasma and/or hypodermis. Target-mediated clearance of gradually released bevacizumab from the hydrogel might contribute to its low bioavailability (Table 1, no. 8 and 13).

### *2.4. Conjugated hydrogel microspheres for anti-TNFα scFv*

The scFv is a fragment of mAb [96] with a MW of about 27 kDa. It consists of variable regions of heavy and light chains connected by a peptide linker [97,98]. Some studies have reported that scFv maintains the binding specificity and potency of the full IgG antibody [97,99]. DLX105 (ESBA105) is a humanized scFv (246 amino acid, MW 26.3 kDa) for human TNFα [99]. The smaller size of scFv

enhances distribution into tissues compared with full-sized mAbs [100] and might enable greater efficacy of scFv especially for the kidney, gastrointestinal tract, pancreas, and skin. On the other hand, scFv lacks FcRn binding and FcRn-mediated recycling and is rapidly eliminated ($t_{1/2}$ of 0.5–2 h), primarily through renal clearance [98,101]. Sustained-release DDS is markedly useful in prolonging the $t_{1/2}$ of scFv and its duration of action and maintaining its primary benefits, namely its great penetration into tissues. In ProLynx β-eliminative DDS, DLX105 was covalently tethered to hydrogel microspheres and gradually released after SC dosing to rats [96].

ProLynx DDS uses self-cleaving β-eliminative linkers for hydrogel cross-linking and drug-conjugation [96–99]. In the linker, the hydroxide ion catalyzes proton removal, the linker-carbamate bond is rapidly cleaved by β-elimination, and the drug and a substituted alkene are released. Electron-withdrawing modulator groups control the pKa of the acidic carbon-hydrogen bond on the α-carbon as well as the drug release rate. Microspheres (40 μm) were prepared using 4-armed PEG (tetra-PEG) terminated with amines and N-hydroxysuccinimide glutarates and a microfluidic device [102] (Figure 3d). The microspheres were bicyclononyne-derivatized and conjugated with azido-linker-DLX105 [96]. Two different modulators were used for the system: the linker for tetra-PEG cross-linking had a longer cleavage $t_{1/2}$ compared with a second linker between the drug and microsphere, so the gels degraded following drug release [96]. The gels released the DLX105 with a short amino-propyl remnant on the N-terminus. $t_{1/2}$ on in vitro release was 11 h at pH 9.4, corresponding to a $t_{1/2}$ of about 1100 h at pH 7.4 at 37 °C. After IV and SC dosing of DLX105 normal solution to rats, $t_{1/2\beta}$ was 4.1 and 3.7 h, respectively (Table 7). The ProLynx gels significantly prolonged $t_{1/2\beta}$ by about 70 times after SC dosing [96] (Table 7).

**Table 7.** Pharmacokinetic parameters of DLX105.

| Formulation | Dosing route | Animal | Dose (nmol/rat) | $C_{max}$ (μM) | $t_{1/2\alpha}$ (h) | $t_{1/2\beta}$ (h) | Relative bioavailability % (vs. IV) | Reference |
|---|---|---|---|---|---|---|---|---|
| Normal solution | IV | rat | ~ 86 | 1.2 | 0.22 | 4.1 | | [96] |
| Normal solution | SC | rat | ~ 86 | 0.12 | - | 3.7 | 100 | [96] |
| ProLynx gel | SC | rat | ~ 57 | 0.0010 | - | 270 | ~ 60 | [96] |

IV: intravenous dosing; SC: subcutaneous dosing; $C_{max}$: maximum concentration; $t_{1/2\alpha}$: half-life during distribution phase; $t_{1/2\beta}$: half-life during terminal elimination phase.

Drug release with the ProLynx DDS is significantly controlled by cleavage of the linkers, and the drug's loading amount, diffusion in DDS, and interactions with polymers consequently make only a minor contribution to the sustained release (Table 1, no. 1–3). The in vivo $t_{1/2\beta}$ of the DLX105 derivative was 4.1-fold faster than that of in vitro release [96]. From data for tetra-PEG microspheres loaded with exenatide, in vivo cleavage is about 3-fold faster than in vitro [103]. Faster in vivo cleavage was also observed in circulating PEG-conjugates containing these linkers; accordingly, the in vivo rate enhancements were not attributable to the SC environment [104]. Moreover, the rates of linker cleavage were the same in the mouse, rat, and monkey [104,105]. On the other hand, catalysis of albumin in β-elimination has been reported for several molecules [106–110]. Lysine (Lys) residues

of albumin, including Lys-199 in subdomain IIA, are thought to cause a general-base effect and catalysis [109,110]. Although albumin concentration is lower in adipose tissue (7.36 mg/mL) than in serum (48.9 mg/mL) [71], a study reported that 0.1 mg/mL BSA catalyzed β-elimination, and 2 mg/mL BSA significantly shortened $t_{1/2\beta}$ of β-elimination from 10 h to 4 min [107]. The study was conducted in vitro at pH 8.8 [107], and the in vivo catalysis of albumin is unclear; however, this might contribute to the shorter $t_{1/2\beta}$ of DLX105 from ProLynx gels (Table 1, no. 8).

The in vivo fate of the gel was evaluated by SC injection of the gel containing no drugs to mice [111] (Table 1, no. 5). After four weeks, the gels were retained in the dosing site, and mild infiltration of inflammatory cells was observed [111]. In another study of repeated SC dosing of placebo gels, slight injection site swelling and moderate SC granulomatous inflammation were observed [103]. These results suggested that APCs may have been involved in the polymer's degradation. The pI of DLX105 has not been published, and the possibility of its interaction with ECM cannot be discussed. However, its small size (MW 26.3 kDa) and short $t_{1/2\beta}$ of the solution on SC dosing (Table 7) suggest a rapid diffusion of DLX105 in hypodermis (Table 1, no. 6). The released DLX105 likely maintained its folding (Table 1, no. 7), which is supported by the finding that DLX105 with a short amino-propyl remnant showed the same bioactivity for TNFα neutralization as free DLX105 [96] and high biocompatibility with the PEG-based hydrogel.

Lymphatic absorption of DLX105 was estimated to be about 80% by linear correlation (Figure 2) and considering its size (MW 26.3 kDa, Table 1, no. 9). In contrast, another study on SC dosing of anti-HER2 scFv with a similar size (MW 27 kDa) reported 10.8% absorption through the lymphatic pathway [112]. Moreover, the SC bioavailability of DLX105 solution, DLX105 ProLynx gel, and anti-HER2 scFv was 100%, 60% [96], and 22% [112], respectively. The anti-HER2 study reported that the simulation was significantly affected by the catabolism of scFv by macrophages in the hypodermis [113]; therefore, the higher bioavailability of DLX105 may be due to higher stability. Based on this assumption, the lower bioavailability of DLX105 ProLynx gel compared with DLX105 solution might be due to a more significant degradation (Table 1, no. 10). As discussed in the preceding sections, the gel gradually released the scFv, and the resulting low hypodermis scFv concentration might result in the degradation of a larger portion of macrophages [113] (Table 1, no. 8). Abundant accumulation of APCs around the ProLynx gel was also related to more significant drug degradation [111,114].

## 3. Intradermal microneedles

Intradermal MN is another DDS for SC sustained release of mAb and proteins [115,116]. The skin is a static barrier that protects internal organs. The stratum corneum of the outermost skin layer is the major hindrance to the penetration of macromolecules into the skin, and only lipophilic small molecules (< 500 Da) can passively diffuse through it. MN arrays consist of multiple protrusions of 25–2000 μm in length, which are long enough to penetrate the stratum corneum [115] (Figure 6). MNs transiently create microscopic aqueous channels and thereby allow mAbs and proteins to bypass the barrier and reach the epidermis and dermis for release. Repair of the microchannels occurs soon after MN removal, avoiding long-term skin damage.

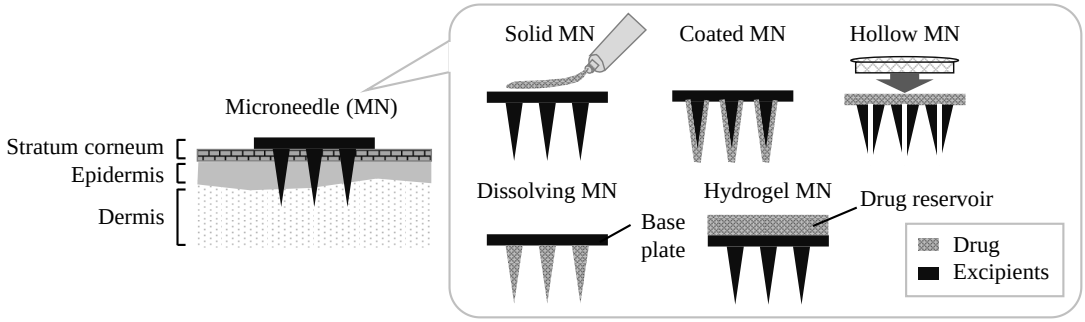


**Figure 6.** Microneedle dosing across the stratum corneum.

MN technologies can be divided into five different categories: solid, coated, hollow, dissolving, and hydrogel [116] (Figure 6). The solid MN is drug-free and is combined with another drug formulation for passive diffusion (patch, solution, cream, or gel). However, the resulting inaccuracy of dosing and the two-step application process are somewhat inconvenient [115]. For coated MNs, drugs are coated on the needle surface; however, drug loading is very low [115] (Figure 6). Hollow MNs are composed of empty cavity needles (5–70 μm wide) that work together with an external auxiliary device (syringe, pump, gas, or electrical assistance) to infuse drug solution through the needles into the skin (Figure 6). The major advantages of hollow MNs are their delivery of a greater volume (10–100 μL/min) of drug solution and precise control at high doses [115,116]. Among the disadvantages, the bulky device might reduce convenience, and the drug flow may be potentially disturbed by the clogging of needle openings with skin tissue or compression of dense dermal tissue. Further, the liquid drug formulations are at risk of stability issues [115,116]. Finally, hollow MNs are rigid and brittle, raising the possibility of the breakage of needles in the skin [117].

**Table 8.** Differences between dissolving and hydrogel microneedles.

| | Dissolving microneedles | Hydrogel microneedles |
|---|---|---|
| Needle tip components | Drug and biodegradable polymer | Only hydrophilic polymer, the drug is in a reservoir attached to the needle array |
| Drug dose | Limited by needle volume | Not limited, loaded in the reservoir. |
| Needle tips after dosing | Dissolve | Not dissolved, swell with skin interstitial fluid |
| Drug release | Rapid | Relatively slow, requires time for swelling and diffusion |
| Polymer deposition in the skin | Have risk | No risk, needles are completely withdrawn |
| Accidental re-piercing | No risk, needles dissolved | No risk, needles are hydrated and swelled |

In dissolving MNs (D-MNs), the needle tips are composed of drugs and cheap biodegradable polymers and are manufactured by a simple process (Figure 6, Table 8). The tips dissolve after application to the skin, and drug release is controlled by the polymer's dissolution rate. Application is

a simple single step, with no risk of accidental re-piercing and no need for sharps disposal [115,116]. A disadvantage is the fact that drug loading is limited by the needle volume [117]. Further, the effects of polymer deposition on the skin should be considered. Taking D-MN of poly(methylvinylether/maleic acid) copolymer as an example, its administration resulted in the deposition of at least 5 mg/cm$^2$ of polymer in the skin [118]. While this is unlikely to be a concern for vaccinations, most mAb and proteins are given by repeated dosing [115]. Careful selection of polymers and their compositions is therefore important, with particular regard to the accumulation, distribution, and elimination of polymers, as well as drug stability and manufacturability [117].

For hydrogel MNs (H-MNs), needles are composed of hydrophilic polymers and contain no drugs; rather, a drug reservoir is attached to the needle array (Figure 6, Table 8). After application to the skin, the needles rapidly absorb skin interstitial fluid and swell to form a hydrogel. This fluid penetrates into the reservoir. The drug dissolves in this fluid and then diffuses through the swollen needles into the skin. Control of the cross-linking density of the needle polymers can be used to adjust the degree of swelling and control drug input rates [115,116]. Fluid uptake of H-MN was 0.9–2.7 μL/h, which is of the same order as hollow MN [119]. The needles are tough and can be completely withdrawn from the skin without deposition. Since swollen needles cannot be re-inserted, there is no risk of re-insertion and no need for sharps disposal [115,116].

Regarding the application of MNs, the skin's viscoelastic property causes force distribution, and some parts of the skin resist deformation [120]. A smaller interspace between needles requires a larger insertion force to pierce the skin [121]. Insertion force depends on the skin's resistance to puncture and its biomechanical properties [120]. Young's modulus of skin increases linearly with age. For children and elderly adults, the elasticity modulus was 70 and 60 N/mm$^2$ (MPa), and skin tension was 21 and 17 N/mm$^2$ (MPa), respectively [122]. The mean ultimate skin deformation before bursting was 75% for newborns and 60% for the elderly. These findings indicate that aging makes the skin thinner, stiffer, less tense, and less flexible [122]. On the other hand, the thickness of the stratum corneum differed among body sites [119,123]. The mean (SD) thickness of the stratum corneum in 71 human volunteers was 18.3 (4.9) μm at the dorsal aspect of the forearm, 11.0 (2.2) μm at the shoulder, and 14.9 (3.4) μm at the buttocks. These findings were positively correlated with pigmentation and were likely attributable to sun exposure [123]. While individual variation was significant, it was much lower than that among body sites. In adults and children, stratum corneum thickness was independent of age and gender [119,123]. Consideration of these variations in the skin is important in MN design and for dosing instructions aimed at delivering stable efficacy and minimizing the adverse effects of mAb and proteins.

### *3.1. Dissolving microneedles for bevacizumab*

Among studies of the sustained release of bevacizumab (anti-VEGF-A IgG1, MW 149 kDa, pI = 8.3) [72], a D-MN has been investigated [124] (Figure 6, Table 8). To prepare the D-MN array, an aqueous solution of polyvinyl alcohol (PVA) (Figure 3e) and bevacizumab was filled onto prefabricated silicone molds, from which the arrays were then removed. The in vitro permeation of bevacizumab across dermatomed neonatal porcine skin on a modified Franz cell apparatus was linearly increased over 0–6 h and reached 9% at 24 h [124]. When this D-MN was applied to rats and held in situ for 24 h, the needles completely dissolved by 24 h. In the PK profile, $C_{max}$ was 6 h, less than the effective concentration; peak/trough ratio ($C_{max}/C_{168\ h}$) was 3.3; and bioavailability was about 0.8% [124] (Table 9). The peak/trough ratio was similar to that with IV dosing (2.7, Table 9), likely due to

the fast release of bevacizumab. The PVA is a hydrophilic polymer and the needles are considered to start to dissolve immediately after insertion. This results in the full available payload of bevacizumab being released from the needle tips as a bolus dose [125] (Table 1, no. 5). The low in vitro permeation of D-MN suggests that only bevacizumab contained in the needles is available for delivery. This is supported by the finding that the in vitro permeated drug amount (9%) was consistent with the needle weight ratio (10%) in the total array [124]. In this preparation method, a part of bevacizumab was contained in the baseplate (Figure 6). In the case of small molecule drugs, a proportion of drugs in the baseplate can permeate through the microchannel; in contrast, the movement of bevacizumab was probably prevented by its large molecular size (Table 1, no. 2). To ensure efficient dosing, the preparation method should be improved such that drug loading is limited to the needles only (Figure 6).

**Table 9.** Pharmacokinetic parameters of bevacizumab after intravenous or transdermal microneedle dosing to rats.

| Formulation | Dosing route | Animal | Dose (mg/head) | $C_{max}$ (μg/mL) | $C_{max}/C_{168\ h}$ | Relative bioavailability % (vs. IV) | References |
|---|---|---|---|---|---|---|---|
| Normal solution | IV | rat | 2.5 | 75.6 | 2.7 | | [124] |
| Dissolving microneedle | transdermal | rat | 5 | 489 | 3.3 | ~ 0.8 | [124] |
| Hydrogel microneedle | transdermal | rat | 5 | 81.2 | 1.4 | ~ 0.2 | [124] |
| Hydrogel microneedle | transdermal | rat | 10 | 358 | 1.7 | ~ 0.8 | [124] |

IV: intravenous dosing; SC: subcutaneous dosing; $C_{max}$: maximum concentration; $C_{max}/C_{168\ h}$: ratio of $C_{max}$ to concentration at 168 h.

### *3.2. Hydrogel microneedles for bevacizumab*

In the study described in Section 3.1, H-MN was also investigated for the sustained release of bevacizumab [72, 124] (Figure 6, Table 8). An aqueous solution of methyl vinyl ether/maleic anhydride copolymer (Gantrez S-97, Figure 3F, 20 wt%), PEG 10000 (7.5 wt%), and $Na_2CO_3$ (3 wt%) was dispensed into the molds and cross-linked. Lyophilized drug reservoirs were separately prepared by dissolving bevacizumab, gelatin, mannitol, NaCl, and sucrose (20 wt%, 10 wt%, 40 wt%, 10 wt%, and 1 wt%, respectively) in water, and the solution was cast into radius cylindrical molds with lyophilization. After lyophilization, the biological activity of bevacizumab was maintained [124]. The in vitro permeation of bevacizumab across porcine skin held in a Franz cell was linearly increased over 0–6 h and reached 24%–28% [124]. After applying the MN to the backs of shaved rats and holding it in situ for 24 h, needles were clearly visible and showed extensive swelling with full dissolution of the reservoirs [124]. Serum concentration after IV dosing of 2.5 mg bevacizumab solution to rats showed a peak/trough ratio ($C_{max}/C_{168\ h}$) of 2.7 (Table 9). Dosing of H-MN containing 5 or 10 mg of drugs showed a smaller $C_{max}$, at 48 h, and a peak/trough ratio of 1.4 and 1.7, respectively [124] (Table 9). H-MN showed prolonged $T_{max}$ and decreased $C_{max}$ compared with D-MN, and the peak/trough ratio was reduced by approximately 50% compared with D-MN and IV dosing, indicating the sustained

absorption of bevacizumab. Serum concentration was lower than the effective concentration, and bioavailability was calculated at about 0.2% and 0.8%, respectively.

The steps for drug release from the H-MN include initial swelling of the array, sufficient diffusion of fluid into the reservoir, dissolution of bevacizumab in the reservoir, and diffusion through the needle into the hypodermis [124] (Table 1, no. 2 and 5). Consistent with these slow steps, H-MN induced sustained in vitro permeation and a slower $T_{max}$ and lower $C_{max}$. The cationic bevacizumab (pI = 8.3) probably interacted with the carboxyl group on the hydrogel polymer of Gantrez S-97 (Table 1, no. 2, Figure 3f), which contributed to the in vitro gradual (6 h) and limited permeation (24%–28%) and the in vivo PK profiles ($T_{max}$, $C_{max}$, peak/trough ratio and the low bioavailability) [72,126]. Since the H-MN was removed at 24 h post-dosing, the $T_{max}$ of 24–48 h indicated a delay in systemic absorption and the possibility that bevacizumab was retained within the skin or lymphatic tissues prior to entry into blood [124]. In turn, these might have been due to the binding of cationic bevacizumab (pI = 8.3) with anionic ECM and slow diffusion due to the large size (MW 149 kDa) [72] (Table 1, no. 6). The possibility that the bevacizumab unfolded was low, owing to the mild MN preparation process and use of lyophilized drug reservoirs and hydrogel needles (Table 1, no. 7).

The lymphatic absorption of bevacizumab (Table 1, no. 9, Figure 2) and its degradation data with lymph node homogenate [28] indicated that APCs in the lymph nodes contributed to degradation (as described in Section 2.3, Table 1, no. 10). Moreover, APCs are recruited around the MN in hypodermis. In another study, MN comprising hyaluronic acid, collagen, and ovalbumin was applied to the skin of mice [127]. Compared with non-treated skin, approximately 10 times more macrophages/monocytes and neutrophils infiltrated into the skin around the MN on the first day after application [127]. As discussed in Section 2.3 above, one possible reason for the sustained absorption and low bioavailability is the degradation of bevacizumab by APCs in hypodermis and/or lymph nodes (Table 1, no. 10). As was also seen with SC V-PEG-V hydrogel dosing, the slow absorption and low bioavailability of H-MN might also be partly attributable to a decrease in FcRn-mediated recycling, increase in FcγR-mediated degradation due to a low drug concentration in hypodermis, and target-mediated clearance (Table 1, no. 8 and 11–13).

Given that the open pores generated by MN treatment might produce complications such as irritation and infection, consideration of pore closure is an important aspect in the selection and design of DDS [119] (Table 1, no. 4). After application of a MN to rats, the defensive properties of skin were re-established within 3–4 h. Complete pore closure was noted by 15 h, but a delay in closure for up to 72 h was also observed due to the incorporation of occlusive materials [128]. Among animals, rat skin has a similar thickness of the stratum corneum, epidermis, and whole skin to human skin, compared with mouse and pig skin [129]. Rat skin significantly differs from human skin in its intercellular lipid composition of the stratum corneum and in its lower corneocyte surface [130] (Table 1, no. 14). Moreover, rat skin is reported to recover more rapidly than human skin after mild alterations in superficial epidermis; the $t_{1/2}$ for the first phase of barrier regeneration for rat and human skin was 19 and 40 h, and recovery of transepidermal water loss was 10 and 30 days, respectively [131] (Table 1, no. 15). A clinical study of MNs demonstrated that microchannel repair and resealing were apparent at 8–24 h post-application, whereas disruption triggered by a 25 G hypodermic needle was significantly notable even after 24 h [132]. In 12 clinical trials, adverse events (erythema, swelling, and bleeding) were related to the MN application site. These were mild and generally disappeared a few hours after application [117]. A clinical study examined the repeated application of an H-MN array to the upper arm of human volunteers every day for a period of 5 days. Neither skin reactions nor disruption of the

skin barrier function were prolonged [133]. These results suggest that MN research has overcome the barrier of species differences and confirmed its applicability to human medication. In addition to increasing the patch size of the safe MN, the design and manufacturing process will be improved to provide higher loading and increase the efficacy of mAb and proteins.

## 4. Conclusions

Antibodies and proteins are critically important modalities. SC sustained-release DDS has the potential to reduce the dosing frequency of these drugs and contribute to the delivery of high value to patients. This article exemplifies several DDS based around polymeric particles, conjugated hydrogel SC injections, and intradermal dissolving/hydrogel MN with four proteins/antibodies (hGH, IFNα-2b, bevacizumab, and scFv). This review suggests that polymers/excipients and manufacturing processes for formulations should be selected with consideration to interactions with drugs, suppression of drug solubility, and maintenance of drug structure/bioactivity. Other important determinants of safe dosing, sustained release, and drug bioavailability include optimization of the size, strength, morphology, and materials of the DDS, polymer deposition, thickness/viscoelastic properties, and regeneration of skin. In the body, many biophysical parameters affect drug PK and the adverse events of DDS, including the small pore size of blood vessels, negative charge of the ECM, concentration of proteins in the hypodermis, recycling of receptors, infiltration of APCs, and degradation by APCs and protease. Although the contribution of each parameter varies among drugs and types of DDS, consideration of these possible factors will lead to the rapid and reliable development of DDS and many long-acting antibody/protein products for patients.

## Use of generative-AI tools declaration

The authors declare they have not used Artificial Intelligence (AI) tools in the creation of this article.

## Acknowledgments

This work was supported by Astellas Pharma Inc.

## Conflict of interest

The authors are employees of Astellas Pharma Inc. The authors declare no conflict of interest.

## Author contributions

The two authors substantially contributed to the conception and design of this manuscript, and the analysis and interpretation of data. The authors drafted this work, reviewed it critically for important intellectual content, and finally approved the version to be published. The authors agree to be accountable for all aspects of this work in ensuring that questions related to the accuracy or integrity of any part of this work are appropriately investigated and resolved.

## References


1. Martin KP, Grimaldi C, Grempler R, et al. (2023) Trends in industrialization of biotherapeutics: a survey of product characteristics of 89 antibody-based biotherapeutics. *MAbs* 15: 2191301. https://doi.org/10.1080/19420862.2023.2191301
2. Shepard HM, Phillips GL, Thanos CD, et al. (2017) Developments in therapy with monoclonal antibodies and related proteins. *Clin Med* 17: 220–232. https://doi.org/10.7861/clinmedicine.17-3-220
3. Lu RM., Hwang YC, Liu IJ, et al. (2020) Development of therapeutic antibodies for the treatment of diseases. *J Biomed Sci* 27: 1. https://doi.org/10.1186/s12929-019-0592-z
4. Zhou Y, Zhang Y, Chen Z, et al. (2024) Dynamic clinical success rates for drugs in the 21st century. *medRxiv*. https://doi.org/10.1101/2024.02.26.24303388
5. Ovacik M, Lin K (2018) Tutorial on monoclonal antibody pharmacokinetics and its considerations in early development. *Clin Transl Sci* 11: 540–552. https://doi.org/10.1111/cts.12567
6. Morales JO, Fathe KR, Brunaugh A, et al. (2017) Challenges and future prospects for the delivery of biologics: oral mucosal, pulmonary, and transdermal routes. *AAPS J* 19: 652–668. https://doi.org/10.1208/s12248-017-0054-z
7. Gill HS, Denson DD, Burris BA, et al. (2008) Effect of microneedle design on pain in human volunteers. *Clin J Pain* 24: 585–594. https://doi.org/10.1097/AJP.0b013e31816778f9
8. Parra A, Hernández C, Prieto-Pinto L (2023) Evaluation of the economic benefits, administration times, and patient preferences associated with the use of biotechnological drugs administered subcutaneously and intravenously in patients with cancer: a systematic review. *Expert Rev Pharmacoecon Outcomes Res* 23: 1017–1026. https://doi.org/10.1080/14737167.2023.2249232
9. Tomasini L, Ferrere M, Nicolas J. (2024) Subcutaneous drug delivery from nanoscale systems. *Nat Rev Bioeng* 2: 501–520. https://doi.org/10.1038/s44222-024-00161-w
10. Epstein RS (2021) Payer perspectives on intravenous versus subcutaneous administration of drugs. *Clinicoecon Outcomes Res* 13: 801–807. https://doi.org/10.2147/CEOR.S317687
11. Anderson KC, Landgren O, Arend RC, et al. (2019) Humanistic and economic impact of subcutaneous versus intravenous administration of oncology biologics. *Future Oncol* 15: 3267–3281. https://doi.org/10.2217/fon-2019-0368
12. Cappuzzo1 F, Zvirbule Z, Korbenfeld EP, et al. (2024) 244mo primary results from imscin002: a study to evaluate patient (pt)- and healthcare professional (hcp)-reported preferences for atezolizumab (atezo) subcutaneous (sc) vs intravenous (iv) for the treatment of NSCLC. *EMBO Open* 9: 102706. https://doi.org/10.1016/j.esmoop.2024.102706
13. Knowles SP, Printz MA, Kang DW, et al. (2021) Safety of recombinant human hyaluronidase ph20 for subcutaneous drug delivery. *Expert Opin Drug Deliv* 18: 1673–1685. https://doi.org/10.1080/17425247.2021.1981286
14. Bittner B, Schmidt J (2024) Advancing subcutaneous dosing regimens for biotherapeutics: clinical strategies for expedited market access. *BioDrugs* 38: 23–46. https://doi.org/10.1007/s40259-023-00626-1
15. Leconet W, Liu H, Guo M, et al. (2018) Anti-PSMA/CD3 bispecific antibody delivery and antitumor activity using a polymeric depot formulation. *Mol Cancer Ther* 17: 1927–1940. https://doi.org/10.1158/1535-7163.MCT-17-1138
16. Kasse CM, Yu AC, Powell AE, et al. (2023) Subcutaneous delivery of an antibody against SARS-CoV-2 from a supramolecular hydrogel depot. *Biomater Sci* 11: 2065–2079. https://doi.org/10.1039/d2bm00819j

17. Van Beers MMC, Slooten C, Meulenaar J, et al. (2017) Micro-flow imaging as a quantitative tool to assess size and agglomeration of PLGA microparticles. *Eur J Pharm Biopharm* 117: 91–104. https://doi.org/10.1016/j.ejpb.2017.04.002
18. Abulateefeh SR (2023) Long-acting injectable PLGA/PLA depots for leuprolide acetate: successful translation from bench to clinic. *Drug Deliv Transl Re* 13: 520–530. https://doi.org/10.1007/s13346-022-01228-0
19. Sali SR, Gondkar SB, Saudagar RB (2018) A review on: atrigel—the magical tool. *Int J Curr Pharm Res* 8: 48–54. https://doi.org/10.22159/ijcpr.2018v10i2.25890
20. Tornøe CW, Agersø H, Nielsen HA, et al. (2004) Population pharmacokinetic modeling of a subcutaneous depot for GnRH antagonist degarelix. *Pharm Res* 21: 574–584. https://doi.org/10.1023/b:pham.0000022403.60314.51
21. Fatima H, Shukrullah S, Hussain H, et al. (2023) Utility of various drug delivery systems and their advantages and disadvantages, In: Singh, R.P., Singh, K.R.B., Singh, J., Adetunji, C.O. Editors, *Nanotechnology for Drug Delivery and Pharmaceuticals*, New York: Academic Press, 235–258. https://doi.org/10.1016/B978-0-323-95325-2.00015-8
22. Hoffman AR, Biller BMK, Cook D, et al. (2005) Efficacy of a long-acting growth hormone (gh) preparation in patients with adult gh deficiency. *J Clin Endocrinol Metab* 90: 6431–6440. https://doi.org/10.1210/jc.2005-0928
23. McKay WF, Peckham SM, Badura JM (2007) A comprehensive clinical review of recombinant human bone morphogenetic protein-2 (INFUSE bone graft). *Int Orthop* 31: 729–734. https://doi.org/10.1007/s00264-007-0418-6
24. Chen Z, Kankala RK, Yang Z, et al. (2022) Antibody-based drug delivery systems for cancer therapy: mechanisms, challenges, and prospects. *Theranostics* 12: 3719–3746. https://doi.org/10.7150/thno.72594
25. Ojaimi YA, Blin T, Lamamy J, et al. (2022) Therapeutic antibodies—natural and pathological barriers and strategies to overcome them. *Pharmacol Ther* 233: 108022. https://doi.org/10.1016/j.pharmthera.2021.108022
26. Swartz MA, Fleury ME (2007) Interstitial flow and its effects in soft tissues. *Annu Rev Biomed Eng* 9: 229–256. https://doi.org/10.1146/annurev.bioeng.9.060906.151850
27. Stader F, Liu C, Derbalah A, et al. (2024) A physiologically based pharmacokinetic model relates the subcutaneous bioavailability of monoclonal antibodies to the saturation of FcRn-mediated recycling in injection-site-draining lymph nodes. *Antibodies (Basel)* 13: 70. https://doi.org/10.3390/antib13030070
28. Wu F, Bhansali SG, Law WC, et al. (2012) Fluorescence imaging of the lymph node uptake of proteins in mice after subcutaneous injection: molecular weight dependence. *Pharm Res* 29: 1843–1853. https://doi.org/10.1007/s11095-012-0708-6
29. Zhong X, Liu Y, Ardekani AM (2024) A compartment model for subcutaneous injection of monoclonal antibodies. *Int J Pharm* 650: 123687. https://doi.org/10.1016/j.ijpharm.2023.123687
30. Datta-Mannan A, Estwick S, Zhou C, et al. (2020) Influence of physiochemical properties on the subcutaneous absorption and bioavailability of monoclonal antibodies. *MAbs* 12: 1770028. https://doi.org/10.1080/19420862.2020.1770028
31. Mieczkowski CA (2023) The evolution of commercial antibody formulations. *J Pharm Sci* 112: 1801–1810. https://doi.org/10.1016/j.xphs.2023.03.026

32. Kinderman F, Yerby B, Jawa V, et al. (2019) Impact of precipitation of antibody therapeutics after subcutaneous injection on pharmacokinetics and immunogenicity. *J Pharm Sci* 108: 1953–1963. https://doi.org/10.1016/j.xphs.2019.01.015
33. Kijanka G, Bee JS, Bishop SM, et al. (2016) Fate of multimeric oligomers, submicron, and micron size aggregates of monoclonal antibodies upon subcutaneous injection in mice. *J Pharm Sci* 105: 1693–1704. https://doi.org/10.1016/j.xphs.2016.02.034
34. Filipe V, Que I, Carpenter JF, et al. (2014) *In vivo* fluorescence imaging of IgG1 aggregates after subcutaneous and intravenous injection in mice. *Pharm Res* 31: 216–227. https://doi.org/10.1007/s11095-013-1154-9
35. Kijanka G, Prokopowicz M, Schellekens H, et al. (2014) Influence of aggregation and route of injection on the biodistribution of mouse serum albumin. *Plos One* 9: e85281. https://doi.org/10.1371/journal.pone.0085281
36. Wang W, Chen N, Shen X, et al. (2012) Lymphatic transport and catabolism of therapeutic proteins after subcutaneous administration to rats and dogs. *Drug Metab Dispos* 40: 952–962. https://doi.org/10.1124/dmd.111.043604
37. Thomas VA, Balthasar JP (2019) Understanding inter-individual variability in monoclonal antibody disposition. *Antibodies (Basel)* 8: 56. https://doi.org/10.3390/antib8040056
38. Richter WF, Bhansali SG, Morris ME (2012) Mechanistic determinants of biotherapeutics absorption following SC administration. *AAPS J* 14: 559–570. https://doi.org/10.1208/s12248-012-9367-0
39. Supersaxo A, Hein WR, Steffen H (1990) Effect of molecular weight on the lymphatic absorption of water-soluble compounds following subcutaneous administration. *Pharm Res* 7: 167–169. https://doi.org/10.1023/a:1015880819328
40. Yang TH, Cleland JL, Lam X, et al. (2000) Effect of zinc binding and precipitation on structures of recombinant human growth hormone and nerve growth factor. *J Pharm Sci* 89: 1480–1485. https://doi.org/10.1002/1520-6017(200011)89:11<1480::aid-jps10>3.0.co;2-m
41. Höybye C (2023) Comparing treatment with daily and long-acting growth hormone formulations in adults with growth hormone deficiency: challenging issues, benefits, and risks. *Best Pract Res Clin Endocrinol Metab* 37: 101788. https://doi.org/10.1016/j.beem.2023.101788
42. Cai Y, Xu M, Yuan M, et al. (2014) Developments in human growth hormone preparations: sustained-release, prolonged half-life, novel injection devices, and alternative delivery routes. *Int J Nanomedicine* 9: 3527–3538. https://doi.org/10.2147/IJN.S63507
43. FDA label, Eli Lilly and Company: Humatrope® somatropin (rDNA origin) for injection vials and cartridges, 2005. Available from: https://www.accessdata.fda.gov/drugsatfda_docs/label/2006/019640s047,019640s052lbl.pdf.
44. Jordan F, Naylor A, Kelly CA, et al. (2010) Sustained release hGH microsphere formulation produced by a novel supercritical fluid technology: *in vivo* studies. *J Control Release* 141: 153–160. https://doi.org/10.1016/j.jconrel.2009.09.013
45. Tracy MA (1998) Development and scale-up of a microsphere protein delivery system. *Biotechnol Prog* 14: 108–115. https://doi.org/10.1021/bp9701271
46. Park K, Skidmore S, Hadar J, et al. (2019) Injectable, long-acting PLGA formulations: analyzing PLGA and understanding microparticle formation. *J Control Release* 304: 125–134. https://doi.org/10.1016/j.jconrel.2019.05.003

47. Oe Y, Kobayashi M, Yoshida T, et al. (2024) Injectable testosterone PLGA microsphere with different characteristics: effect of preparation method (paddle mixing versus microfluidic device). *Pharm Dev Technol* 29: 482–491. https://doi.org/10.1080/10837450.2024.2348580
48. Kojima R, Yoshida T, Tasaki H, et al. (2015) Release mechanisms of tacrolimus-loaded PLGA and PLA microspheres and immunosuppressive effects of the microspheres in a rat heart transplantation model. *Int J Pharm* 492: 20–27. https://doi.org/10.1016/j.ijpharm.2015.07.004
49. van de Weert M, Hoechstetter J, Hennink WE, et al. (2000) The effect of a water/organic solvent interface on the structural stability of lysozyme. *J Control Release* 68: 351–359. https://doi.org/10.1016/s0168-3659(00)00277-7
50. Su Y, Zhang B, Sun R, et al. (2021) PLGA-based biodegradable microspheres in drug delivery: recent advances in research and application. *Drug Deliv* 28: 1397–1418. https://doi.org/10.1080/10717544.2021.1938756
51. FDA label, Genentech, Inc.: Nutropin Depot® somatropin (rDNA origin) for injectable suspension, 1999. Available from: https://www.accessdata.fda.gov/drugsatfda_docs/label/2004/21075s008lbl.pdf.
52. Kemp SF, Fielder PJ, Attie KM, et al. (2004) Pharmacokinetic and pharmacodynamic characteristics of a long-acting growth hormone (GH) preparation (nutropin depot) in GH-deficient children. *J Clin Endocrinol Metab* 89: 3234–3240. https://doi.org/10.1210/jc.2003-030825
53. Shive MS, Anderson JM (1997) Biodegradation and biocompatibility of PLA and PLGA microspheres. *Adv Drug Deliv Rev* 28: 5–24. https://doi.org/10.1016/s0169-409x(97)00048-3
54. Zhang H, Yang Z, Wu D, et al. (2023) The effect of polymer blends on the *in vitro* release/degradation and pharmacokinetics of moxidectin-loaded PLGA microspheres. *Int J Mol Sci* 24: 14729. https://doi.org/10.3390/ijms241914729
55. Shah VR, Gupta PK (2018) Structural stability of recombinant human growth hormone (r-hGH) as a function of polymer surface properties. *Pharm Res* 35: 98. https://doi.org/10.1007/s11095-018-2372-y
56. Bosquillon C, Préat V, Vanbever R (2004) Pulmonary delivery of growth hormone using dry powders and visualization of its local fate in rats. *J Control Release* 96: 233–244. https://doi.org/10.1016/j.jconrel.2004.01.027
57. Patton JS, McCabe JG, Hansen SE, et al. (1989) Absorption of human growth hormone from the rat lung. *Biotechnol Ther* 1 :213–228.
58. Shive MS, Anderson JM (1997) Biodegradation and biocompatibility of PLA and PLGA microspheres. *Adv Drug Deliv Rev* 28: 5–24. https://doi.org/10.1016/s0169-409x(97)00048-3
59. Ningrum RA (2014) Human interferon alpha-2b: a therapeutic protein for cancer treatment. *Scientifica (Cairo)*: 970315. https://doi.org/10.1155/2014/970315
60. Radwanski E, Perentesis G, Jacobs S, et al. (1987) Pharmacokinetics of interferon alpha-2b in healthy volunteers. *J Clin Pharmacol* 27: 432–435. https://doi.org/10.1002/j.1552-4604.1987.tb03044.x
61. Li Z, Li L, Liu Y, et al. (2011) Development of interferon alpha-2b microspheres with constant release. *Int J Pharm* 410: 48–53. https://doi.org/10.1016/j.ijpharm.2011.03.016
62. Chan Y-P, Meyrueix R, Kravtzoff R, et al. (2007) Review on Medusa®: a polymer-based sustained release technology for protein and peptide drugs. *Expert Opin Drug Deliv* 4: 441–451. https://doi.org/10.1517/17425247.4.4.441

63. Trépo C, Meyrueix R, Maynard M, et al. (2006) Novel sustained release formulation of IFNα-2b improves tolerability and demonstrates potent viral load reduction in a phase I/II HCV clinical trial. *J Clin Virol* 36: S24. https://doi.org/10.1016/S1386-6532(06)80081-8
64. Bonnet-Gonnet C, Chognot D, Soula O, et al. (2014) Pharmaceutical formulations for the prolonged release of active principle(s), and their applications, especially therapeutic applications. *US Patent*: 8679540 B2
65. Hill CP, Osslund TD, Eisenberg D (1993) The structure of granulocyte-colony-stimulating factor and its relationship to other growth factors. *Proc Natl Acad Sci USA* 90: 5167–5171. https://doi.org/10.1073/pnas.90.11.5167
66. Nagabhushan TL, Reichert P, Walter MR, et al. (2011) Type I interferon structures: possible scaffolds for the interferon-alpha receptor complex. *Can J Chem* 80: 1166–1173. https://doi.org/10.1139/v02-158
67. Chino M, Maglio O, Nastri F, et al. (2015) Artificial diiron enzymes with a de novo designed four-helix bundle structure. *Eur J Inorg Chem* 21: 3371–3390. https://doi.org/10.1002/ejic.201500470
68. Schaefer MH, Wanker EE, Andrade-Navarro MA (2012) Evolution and function of CAG/polyglutamine repeats in protein-protein interaction networks. *Nucleic Acids Res* 40: 4273–4287. https://doi.org/10.1093/nar/gks011
69. Jakubek RS, Workman RJ, White SE, et al. (2019) Polyglutamine solution-state structural propensity is repeat length dependent. *J Phys Chem B* 123: 4193–4203. https://doi.org/10.1021/acs.jpcb.9b01433
70. Rathod S, Bahadur P, Tiwari S (2021) Nanocarriers based on vitamin E-TPGS: Design principle and molecular insights into improving the efficacy of anticancer drugs. *Int J Pharm* 592: 120045. https://doi.org/10.1016/j.ijpharm.2020.120045
71. Ellmerer M, Schaupp L, Brunner GA, et al. (2000) Measurement of interstitial albumin in human skeletal muscle and adipose tissue by open-flow microperfusion. *Am J Physiol Endocrinol Metab* 278: E352–356. https://doi.org/10.1152/ajpendo.2000.278.2.E352
72. Kaja S, Hilgenberg JD, Everett E, et al. (2011) Effects of dilution and prolonged storage with preservative in a polyethylene container on Bevacizumab (Avastin™) for topical delivery as a nasal spray in anti-hereditary hemorrhagic telangiectasia and related therapies. *Hum Antibodies* 20: 95–101. https://doi.org/10.3233/HAB-2011-0244
73. Elebiyo TC, Rotimi D, Evbuomwan IO, et al. (2022) Reassessing vascular endothelial growth factor (VEGF) in anti-angiogenic cancer therapy. *Cancer Treat Res Commun* 32: 100620. https://doi.org/10.1016/j.ctarc.2022.100620
74. Lu JF, Bruno R, Eppler S, et al. (2008) Clinical pharmacokinetics of bevacizumab in patients with solid tumors. *Cancer Chemoth Pharm* 62: 779–786. https://doi.org/10.1007/s00280-007-0664-8
75. Lee ALZ, Ng VWL, Gao S, et al. (2015) Injectable biodegradable hydrogels from vitamin D-functionalized polycarbonates for the delivery of avastin with enhanced therapeutic efficiency against metastatic colorectal cancer. *Biomacromolecules* 16: 465–475. https://doi.org/10.1021/bm5015206
76. Fletcher NA, Krebs MD (2018) Sustained delivery of anti-VEGF from injectable hydrogel systems provides a prolonged decrease of endothelial cell proliferation and angiogenesis *in vitro*. *RSC Adv* 8: 8999–9005. https://doi.org/10.1039/c7ra13014g

77. Courtenay AJ, McCrudden MTC, McAvoy KJ, et al. (2018) Microneedle-mediated transdermal delivery of bevacizumab. *Mol Pharm* 15: 3545–3556. https://doi.org/10.1021/acs.molpharmaceut.8b00544
78. Huynh V, Wylie RG (2019) Displacement affinity release of antibodies from injectable hydrogels. *ACS Appl Mater Interfaces* 11: 30648–30660. https://doi.org/10.1021/acsami.9b12572
79. Gregoritza M, Messmann V, Abstiens K, et al. (2017) Controlled antibody release from degradable thermoresponsive hydrogels cross-linked by Diels-Alder chemistry. *Biomacromolecules* 18: 2410–2418. https://doi.org/10.1021/acs.biomac.7b00587
80. Huynh V, Wylie RG (2018) Competitive affinity release for long-term delivery of antibodies from hydrogels. *Angew Chem Int Ed Engl* 57: 3406–3410. https://doi.org/10.1002/anie.201713428
81. Lin YS, Nguyen C, Mendoza JL, et al. (1999) Preclinical pharmacokinetics, interspecies scaling, and tissue distribution of a humanized monoclonal antibody against vascular endothelial growth factor. *J Pharmacol Exp Ther* 288: 371–378.
82. Lee ALZ, Ng VWL, Poon GL, et al. (2015) Co-delivery of antiviral and antifungal therapeutics for the treatment of sexually transmitted infections using a moldable, supramolecular hydrogel. *Adv Healthc Mater* 4: 385–394. https://doi.org/10.1002/adhm.201400340
83. Ghosh I, Gutka H, Krause ME, et al. (2023) A systematic review of commercial high concentration antibody drug products approved in the US: formulation composition, dosage form design and primary packaging considerations. *MAbs* 15: 2205540. https://doi.org/10.1080/19420862.2023.2205540
84. Yang C, Lee A, Gao S, et al. (2019) Hydrogels with prolonged release of therapeutic antibody: Block junction chemistry modification of 'ABA' copolymers provides superior anticancer efficacy. *J Control Release* 293: 193–200. https://doi.org/10.1016/j.jconrel.2018.11.026
85. Kyriakides TR, Kim HJ, Zheng C, et al. (2022) Foreign body response to synthetic polymer biomaterials and the role of adaptive immunity. *Biomed Mater* 17: 022007. https://doi.org/10.1088/1748-605X/ac5574
86. Challa DK, Wang X, Montoyo HP, et al. (2019) Neonatal Fc receptor expression in macrophages is indispensable for IgG homeostasis. *MAbs* 11: 848–860. https://doi.org/10.1080/19420862.2019.1602459
87. Stader F, Liu C, Derbalah A, et al. (2024) A physiologically based pharmacokinetic model relates the subcutaneous bioavailability of monoclonal antibodies to the saturation of FcRn-mediated recycling in injection-site-draining lymph nodes. *Antibodies (Basel)* 13: 70. https://doi.org/10.3390/antib13030070
88. Davis JD, Padros MB, Conrado DJ, et al. (2024) Subcutaneous administration of monoclonal antibodies: pharmacology, delivery, immunogenicity, and learnings from applications to clinical development. *Clin Pharmacol Ther* 115: 422–439. https://doi.org/10.1002/cpt.3150
89. Mould DR, Baumann A, Kuhlmann J, et al. (2007) Population pharmacokinetics-pharmacodynamics of alemtuzumab (Campath) in patients with chronic lymphocytic leukaemia and its link to treatment response. *Br J Clin Pharmacol* 64: 278–291. https://doi.org/10.1111/j.1365-2125.2007.02914.x
90. Gibbs JP, Doshi S, Kuchimanchi M, et al. (2017) Impact of target-mediated elimination on the dose and regimen of evolocumab, a human monoclonal antibody against proprotein convertase subtilisin/kexin type 9 (PCSK9). *J Clin Pharmacol* 57: 616–626. https://doi.org/10.1002/jcph.840

91. Rudnick SI, Lou J, Shaller CC, et al. (2011) Influence of affinity and antigen internalization on the uptake and penetration of anti-HER2 antibodies in solid tumors. *Cancer Res* 71: 2250–2259. https://doi.org/10.1158/0008-5472.CAN-10-2277
92. Finley SD, Dhar M, Popel AS (2013) Compartment model predicts VEGF secretion and investigates the effects of VEGF trap in tumor-bearing mice. *Front Oncol* 3: 196. https://doi.org/10.3389/fonc.2013.00196
93. Ng CM, Fielder PJ, Jin J, et al. (2016) Mechanism-based competitive binding model to investigate the effect of neonatal Fc receptor binding affinity on the pharmacokinetic of humanized anti-VEGF monoclonal IgG1 antibody in cynomolgus monkey. *AAPS J* 18: 948–959. https://doi.org/10.1208/s12248-016-9911-4
94. Keyes KA, Mann L, Sherman M, et al. (2004) LY317615 decreases plasma VEGF levels in human tumor xenograft-bearing mice. *Cancer Chemother Pharmacol* 53: 133–140. https://doi.org/10.1007/s00280-003-0713-x
95. van Bueren JJL, Bleeker WK, Bøgh HO, et al. (2006) Effect of target dynamics on pharmacokinetics of a novel therapeutic antibody against the epidermal growth factor receptor: implications for the mechanisms of action. *Cancer Res* 66: 7630–7638. https://doi.org/10.1158/0008-5472.CAN-05-4010
96. Schneider EL, Hearn BR, Pfaff SJ, et al. (2016) Approach for half-Life extension of small antibody fragments that does not affect tissue uptake. *Bioconjug Chem* 27: 2534–2539. https://doi.org/10.1021/acs.bioconjchem.6b00469
97. Ottiger M, Thiel MA, Feige U, et al. (2009) Efficient intraocular penetration of topical anti-TNF-alpha single-chain antibody (ESBA105) to anterior and posterior segment without penetration enhancer. *Invest Ophthalmol Vis Sci* 50: 779–786. https://doi.org/10.1167/iovs.08-2372
98. Muñoz-López P, Ribas-Aparicio RM, Becerra-Báez EI, et al. (2022) Single-chain fragment variable: recent progress in cancer diagnosis and therapy. *Cancers (Basel)* 14: 4206. https://doi.org/10.3390/cancers14174206
99. Furrer E, Berdugo M, Stella C, et al. (2009) Pharmacokinetics and posterior segment biodistribution of ESBA105, an anti-TNF-alpha single-chain antibody, upon topical administration to the rabbit eye. *Invest Ophthalmol Vis Sci* 50: 771–778. https://doi.org/10.1167/iovs.08-2370
100. Li Z, Krippendorff BF, Sharma S, et al. (2016) Influence of molecular size on tissue distribution of antibody fragments. *mAbs* 8: 113–119. https://doi.org/10.1080/19420862.2015.1111497
101. Knowles SM, Wu AM (2012) Advances in immuno-positron emission tomography: antibodies for molecular imaging in oncology. *J Clin Oncol* 30: 3884–3892. https://doi.org/10.1200/JCO.2012.42.4887
102. Sakai T, Matsunaga T, Yamamoto Y, et al. (2008) Design and fabrication of a high-strength hydrogel with ideally homogeneous network structure from tetrahedron-like macromonomers. *Macromolecules* 41: 5379–5384. https://doi.org/10.1021/ma800476x
103. Schneider EL, Henise J, Reid R, et al. (2016) Hydrogel drug delivery system using self-cleaving covalent linkers for once-a-week administration of exenatide. *Bioconjug Chem* 27: 1210–1215. https://doi.org/10.1021/acs.bioconjchem.5b00690
104. Santi DV, Schneider EL, Reid R, et al. (2012) Predictable and tunable half-life extension of therapeutic agents by controlled chemical release from macromolecular conjugates. *Proc Natl Acad Sci U S A* 109: 6211–6216. https://doi.org/10.1073/pnas.1117147109

105. Santi DV, Schneider EL, Ashley GW (2014) Macromolecular prodrug that provides the irinotecan (CPT-11) active-metabolite SN-38 with ultralong half-life, low C(max), and low glucuronide formation. *J Med Chem* 57: 2303–2314. https://doi.org/10.1021/jm401644v
106. Deb T, Tu J, Franzini RM (2021) Mechanisms and substituent effects of metal-free bioorthogonal reactions. *Chem Rev* 121: 6850–6914. https://doi.org/10.1021/acs.chemrev.0c01013
107. Klein G, Reymond JL (1998) An enantioselective fluorimetric assay for alcohol dehydrogenases using albumin-catalyzed beta-elimination of umbelliferone. *Bioorg Med Chem Lett* 8: 1113–1116. https://doi.org/10.1016/s0960-894x(98)00165-6
108. Tu J, Xu M, Parvez S, et al. (2018) Bioorthogonal removal of 3-isocyanopropyl groups enables the controlled release of fluorophores and drugs *in vivo*. *J Am Chem Soc* 140: 8410–8414. https://doi.org/10.1021/jacs.8b05093
109. Roller SG, Dieckhaus CM, Santos WL, et al. (2002) Interaction between human serum albumin and the felbamate metabolites 4-hydroxy-5-phenyl-[1,3]oxazinan-2-one and 2-phenylpropenal. *Chem Res Toxicol* 15: 815–824. https://doi.org/10.1021/tx025509h
110. Xu M, Deb T, Tu J, et al. (2019) Tuning isonitrile/tetrazine chemistry for accelerated deprotection and formation of stable conjugates. *J Org Chem* 84: 15520–15529. https://doi.org/10.1021/acs.joc.9b02522
111. Sakai T, Fujiyabu T (2020) Control over swelling of injectable gel, In: Sakai, T. Editor, *Physics of Polymer Gels*, Weinheim: Wiley-VCH, 261–276. https://doi.org/10.1002/9783527346547.ch17
112. Li Z, Yu X, Li Y, et al. (2021) A two-pore physiologically based pharmacokinetic model to predict subcutaneously administered different-size antibody/antibody fragments. *AAPS J* 23: 62. https://doi.org/10.1208/s12248-021-00588-8
113. Richter WF, Christianson GJ, Frances N, et al. (2018) Hematopoietic cells as site of first-pass catabolism after subcutaneous dosing and contributors to systemic clearance of a monoclonal antibody in mice. *mAbs* 10: 803–813. https://doi.org/10.1080/19420862.2018.1458808
114. Hangasky JA, Chen W, Dubois SP, et al. (2022) A very long-acting IL-15: implications for the immunotherapy of cancer. *J Immunother Cancer* 10: e004104. https://doi.org/10.1136/jitc-2021-004104
115. Kirkby M, Hutton ARJ, Donnelly RF (2020) Microneedle mediated transdermal delivery of protein, peptide and antibody based therapeutics: current status and future considerations. *Pharm Res* 37: 117. https://doi.org/10.1007/s11095-020-02844-6
116. Zhao J, Xu G, Yao X, et al. (2022) Microneedle-based insulin transdermal delivery system: current status and translation challenges. *Drug Deliv Transl Res* 12: 2403–2427. https://doi.org/10.1007/s13346-021-01077-3
117. Zhang J, Li H, Albakr L, et al. (2023) Microneedle-enabled therapeutics delivery and biosensing in clinical trials. *J Control Release* 360: 687–704. https://doi.org/10.1016/j.jconrel.2023.07.023
118. McCrudden MTC, Alkilani AZ, McCrudden CM, et al. (2014) Design and physicochemical characterisation of novel dissolving polymeric microneedle arrays for transdermal delivery of high dose, low molecular weight drugs. *J Control Release* 180: 71–80. https://doi.org/10.1016/j.jconrel.2014.02.007
119. Duarah S, Sharma M, Wen J (2019) Recent advances in microneedle-based drug delivery: Special emphasis on its use in paediatric population. *Eur J Pharm Biopharm* 136: 48–69. https://doi.org/10.1016/j.ejpb.2019.01.005
120. Kashaninejad N, Munaz A, Moghadas H, et al. (2021) Microneedle arrays for sampling and sensing skin interstitial fluid. *Chemosensors* 9: 83. https://doi.org/10.3390/chemosensors9040083

121. Olatunji O, Das DB, Garland MJ, et al. (2013) Influence of array interspacing on the force required for successful microneedle skin penetration: theoretical and practical approaches. *J Pharm Sci* 102: 1209–1221. https://doi.org/10.1002/jps.23439
122. Pawlaczyk M, Lelonkiewicz M, Wieczorowski M (2013) Age-dependent biomechanical properties of the skin. *Postepy Dermatol Alergol* 30: 302–306. https://doi.org/10.5114/pdia.2013.38359
123. Sandby-Møller J, Poulsen T, Wulf HC (2003) Epidermal thickness at different body sites: relationship to age, gender, pigmentation, blood content, skin type and smoking habits. *Acta Derm Venereol* 83: 410–413. https://doi.org/10.1080/00015550310015419
124. Courtenay AJ, McCrudden MTC, McAvoy KJ, et al. (2018) Microneedle-mediated transdermal delivery of bevacizumab. *Mol Pharm* 15: 3545–3556. https://doi.org/10.1021/acs.molpharmaceut.8b00544
125. Amodwala S, Kumar P, Thakkar HP (2017) Statistically optimized fast dissolving microneedle transdermal patch of meloxicam: a patient friendly approach to manage arthritis. *Eur J Pharm Sci* 104: 114–123. https://doi.org/10.1016/j.ejps.2017.04.001
126. Hutton ARJ, Kirkby M, Bogaert TV, et al. (2024) Transdermal administration of nanobody molecules using hydrogel-forming microarray patch technology: a unique delivery approach. *Macromol Mater Eng* 309: 2400029. https://doi.org/10.1002/mame.202400029
127. Hirobe S, Susai R, Takeuchi H, et al. (2021) Characteristics of immune induction by transcutaneous vaccination using dissolving microneedle patches in mice. *Int J Pharm* 601: 120563. https://doi.org/10.1016/j.ijpharm.2021.120563
128. Kalluri H, Banga AK (2011) Formation and closure of microchannels in skin following microporation. *Pharm Res* 28: 82–94. https://doi.org/10.1007/s11095-010-0122-x
129. Jung EC, Maibach HI (2015) Animal models for percutaneous absorption. *J Appl Toxicol* 35: 1–10. https://doi.org/10.1002/jat.3004
130. Capt A, Luzy AP, Esdaile D, et al. (2007) Comparison of the human skin grafted onto nude mouse model with *in vivo* and *in vitro* models in the prediction of percutaneous penetration of three lipophilic pesticides. *Regul Toxicol Pharmacol* 47: 274–287. https://doi.org/10.1016/j.yrtph.2006.11.008
131. Scott RC, Dugard PH, Doss AW (1986) Permeability of abnormal rat skin. *J Invest Dermatol* 86: 201–207. https://doi.org/10.1111/1523-1747.ep12284280
132. Haq MI, Smith E, John DN, et al. (2009) Clinical administration of microneedles: skin puncture, pain and sensation. *Biomed Microdevices* 11: 35–47. https://doi.org/10.1007/s10544-008-9208-1
133. Al-Kasasbeh R, Brady AJ, Courtenay AJ, et al. (2020) Evaluation of the clinical impact of repeat application of hydrogel-forming microneedle array patches. *Drug Deliv Transl Res* 10: 690–705. https://doi.org/10.1007/s13346-020-00727-2


AIMS Press